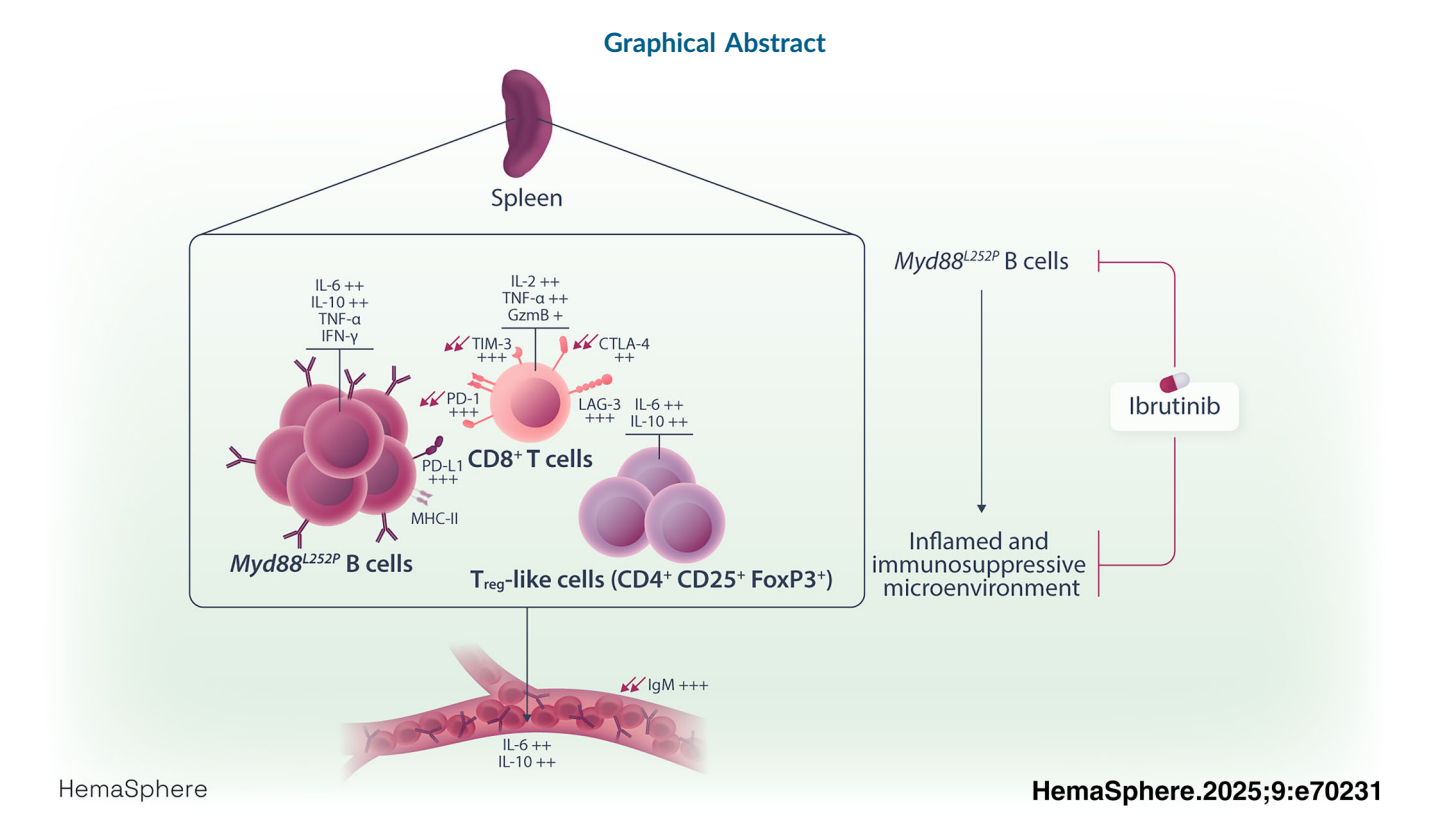
### ARTICLE

## HemaSphere Seha

Check for updates

Uncovering regulatory B-cell features associated with regulatory T-cell expansion and global T-cell exhaustion in Waldenström macroglobulinemia *Myd88*<sup>L252P</sup>-like lymphoplasmacytic lymphomas

Quentin Lemasson<sup>1,^</sup> | Maxime Tabaud<sup>1,^</sup> | Ophélie Téteau<sup>1</sup> | Bastien Carle<sup>1</sup> | Mina Chabaud<sup>1</sup> | Jean Feuillard<sup>1,2</sup> | Nathalie Faumont<sup>1</sup> | Christelle Vincent-Fabert<sup>1</sup>



### ARTICLE

# HemaSphere Seha



25729241, 2025, 10, Downloaded from https://onlinelibrary.wiley.com/doi/10.1002/hem3.70231, Wiley Online Library on [03/11/2025]. See the Terms and Conditions (https://onlinelibrary.wiley.com/terms-and-conditions) on Wiley Online Library for rules of use; OA articles are governed by the applicable Creative Commons Licenseaux.

### Uncovering regulatory B-cell features associated with regulatory T-cell expansion and global T-cell exhaustion in Waldenström macroglobulinemia Myd88<sup>L252P</sup>-like lymphoplasmacytic lymphomas

Quentin Lemasson<sup>1,^</sup> | Maxime Tabaud<sup>1,^</sup> | Ophélie Téteau<sup>1</sup> | Bastien Carle<sup>1</sup> | Jean Feuillard<sup>1,2</sup> | Nathalie Faumont<sup>1</sup> | Christelle Vincent-Fabert<sup>1</sup> Mina Chabaud<sup>1</sup>

Correspondence: Christelle Vincent-Fabert (christelle.vincent-fabert@unilim.fr)

#### **Abstract**

Waldenström's macroglobulinemia (WM) is a rare, indolent lymphoproliferative disorder, genetically characterized by the presence of the L265P mutation in the MYD88 gene in almost all cases, resulting in constitutive activation of NF-kappa B (NF-κB). Despite its slow progression, WM remains incurable due to the lack of specific treatments. The efficacy of therapies capable of reactivating the antitumor response of T-cells is well documented in various solid tumors. Apart from Hodgkin's lymphoma, these therapies have very mixed effects on B-cell lymphomas, especially those with NF-kB activation. Here, we used the published Myd88<sup>L252P</sup> mouse model, which develops a WM-like disease close to human WM. By focusing on T-cell exhaustion and regulatory T-cell expansion, we show how T-cells located near WM-like tumors in mice are disrupted, while Myd88<sup>L252P</sup> tumor B-cells adopt an immunoregulatory phenotype evoking regulatory B-cells. We also demonstrate, for the first time in the context of WM, the dual effect of Ibrutinib, an irreversible inhibitor of Bruton's tyrosine kinase (BTK), able to decrease B-cell activation and expansion and to partially reverse T-cell depletion in Myd88<sup>L252P</sup> mice. With Ibrutinib as an example, this work provides new perspectives for the development of therapeutic combinations targeting tumor B-cells while reactivating antitumor T-cells.

#### INTRODUCTION

Waldenström's disease (WM), described by Jan G. Waldenström in 1944, is an incurable, indolent lymphoplasmacytic lymphoma (LPL) of the elderly that accounts for less than 5% of B-cell lymphomas. This slowly evolving lymphoma is characterized by expansion of a lymphoplasmacytic clone of medullary localization with secretion of a monoclonal immunoglobulin type M (IgM). Being specific of WM, clonal cells show continuous differentiation between the small mature lymphocyte and the mature plasma cell (PC). This unique characteristic may be used as a biological marker for WM diagnosis by evidencing the B-cell clonality in both lymphocytes and plasma cells by flow cytometry. Similar to other lymphomas, cytogenetic and molecular abnormalities have been identified and can aid diagnosis and be used as prognostic factors. The main chromosomal aberrations are 6q deletions (in 20%-40% of patients), 13q deletions (10%-15%), trisomy 18 (10%), trisomy 4, and 17p deletions (8%).<sup>2</sup> The discovery

of the L265P mutation in MYD88, originally described in Diffuse Large B-Cell Lymphoma (DLBCL), in over 90% of WM patients has demonstrated that WM is a genuine genetically distinct entity from other indolent IgM-secreting lymphomas.<sup>3-5</sup> Indeed, WM is the only entity to be associated with an activating mutation of MYD88 (MYD88 L265P, the most frequent) in more than 90% of cases. Another frequent mutation, almost specific of WM, is the WHIM-like mutation of CXCR4 (30% of WM patients), which results in the lack of desensitization of this receptor, which would explain why WM B-cells are prone to home in the bone marrow.<sup>6</sup>

Despite current progress and development of targeted therapies such as Bruton's tyrosine kinase inhibitors (BTKi) and, to a less extent, Bcl2 inhibitors, WM still remains incurable. It is therefore important to develop new approaches in this field. Until recently, adequate preclinical models, which is an important step toward the development of these new approaches, were lacking. Like a few other groups, we have created an animal model with B-cell specific expression of

This is an open access article under the terms of the Creative Commons Attribution-NonCommercial-NoDerivs License, which permits use and distribution in any medium, provided the original work is properly cited, the use is non-commercial and no modifications or adaptations are made. © 2025 The Author(s). HemaSphere published by John Wiley & Sons Ltd on behalf of European Hematology Association.

<sup>&</sup>lt;sup>1</sup>UMR CNRS7276, Inserm1262, University of Limoges: Contrôle de la Réponse Immune B et des Lymphoproliférations, Team 1, 2MB2C: Molecular Mechanisms of B Cell Cancerogenesis, Limoges, France

<sup>&</sup>lt;sup>2</sup>Hematology Laboratory of Dupuytren Hospital University Center (CHU) of Limoges, Limoges, France

Quentin Lemasson and Maxime Tabaud are co-first authors.

HemaSphere 3 of 17

the mutated form of *Myd88*.<sup>8-11</sup> Compared to others, our mouse model recapitulates the main features of WM.<sup>11,12</sup> Indeed, our *Myd88*<sup>L252P</sup> mouse model develops at 9–12 months of age (i) an indolent, (ii) lymphoplasmacytic B-cell lymphoma in the spleen (iii) with, in the blood, secretion of a monoclonal IgM, and (iv) a lymphoplasmocytic B-cell expansion in the bone marrow. This is a unique opportunity to both understand how *Myd88*<sup>L252P</sup> induces WM and to identify new therapeutic perspectives.

Like in other cancers, escape from the immune response is a crucial step in the emergence of lymphomas, especially for those with NF-κB activation. 13-16 Cancer cells often reprogram the tumor microenvironment (TME) to protect themselves from the immune defenses of the host. Among the mechanisms of escape from the immune response, T-cell exhaustion through overexpression of immune checkpoints and/or secretion of immunosuppressive cytokines are usually reported, including in most B-cell lymphomas. 17-21 For example, DLBCLs are associated with 9g amplification in 11% of cases, leading to overexpression of CD274/PD-L1 by tumor cells.<sup>22</sup> The MYD88<sup>L265P</sup> mutation has also been associated with PD-L1 overexpression.<sup>23</sup> However, apart from Hodgkin lymphomas, therapies aiming to restore the antitumor immune response in B-cell lymphomas had very mitigated effects. Knowing the pathways deregulated in WM like TLR/NF-κB, JAK/STAT, BCR, and PI3K/AKT signaling, which we showed to be responsible for PD-L1 overexpression<sup>15</sup> and their consequences in terms of cytokine secretion, the WM tumor microenvironment should be disturbed. In 2013. Grote et al. showed for the first time that PD-L1 and PD-L2 are overexpressed not only on the surface of WM tumor cells but also on the surface of cells in the tumor microenvironment, promoting their proliferation.<sup>24</sup> In 2018, Jalali et al. showed in patients that CD19<sup>+</sup>CD138<sup>+</sup> WM cells overexpress and secrete large amounts of PD-1 ligands (PD-L1 and PD-L2), which can be found in the blood and the bone marrow. Moreover, T-cells cultured in the presence of serum from WM patients had their proliferation severely compromised.<sup>25</sup> In 2021 and 2022, two reports presented results on the immune microenvironment in WM, demonstrating that immune escape has to take place in the clonal emergence and progression of WM.<sup>26,27</sup> While these studies are promising in terms of their therapeutic potential, they remain to be confirmed, and they raise the question of the exact mechanisms involved. To this end, we studied the immune microenvironment of WM-like tumors in the Myd88<sup>L252P</sup> mouse model. Our results uncover the existence of several immune escape aspects in Myd88-driven lymphoplasmacytic lymphoma. Our results also indicate that therapeutic effects of the Bruton's tyrosine kinase inhibitor (BTKi) Ibrutinib are associated with its capability to restore the T-cell immune response.

#### MATERIALS AND METHODS

#### Mouse model

The  $Myd88^{L252P}$ - $Cd19^{Cre}$  mouse model has been previously described. <sup>11</sup> For B-cell expression of the transgene,  $Myd88^{L252P}$  tg/tg animals (C57Bl6/J genetic background) were crossed with  $Cd19^{Cre}$  tg/tg mice (Balb/c background). The animals used in this study are  $Myd88^{L252P}$  tg/tg- $Cd19^{Cre}$  tg/tg. These mice will hereafter be referred to as  $Myd88^{L252P}$  mice. Animals were housed at 21–23°C with a 12-h light/dark cycle. All procedures were conducted under an approved protocol according to European guidelines for animal experimentation (French national authorization number: 8708503 and French ethics committee registration number APAFIS #52230-2024112911138557 v3).

#### Sera analyses

Serum was obtained from blood collected retro-orbitally after centrifugation (20 min, 3000 rpm). The serum electrophoresis assay and specific ELISA for IgM secretion were performed as previously described.  $^{28,29}$ 

#### Flow cytometry

Bone marrow and spleen cells from  $Cd19^{Cre}$  and  $Myd88^{L252P}$  were collected as previously described. <sup>11</sup> Cell suspensions were resuspended at 4°C in a labeling buffer (phosphate-buffered saline [PBS], 1% BSA, 2 mM EDTA) and labeled with fluorescent-conjugated monoclonal antibodies listed in the Supporting Information S2: Materials and Methods. The "Mouse Tregs detection kit" (Miltenyi Biotec®) was used for regulatory T-cell staining. Membrane labeling (CD4 2  $\mu$ L + CD25 2  $\mu$ L, 20 min at 4°C) was performed on 1 million cells. Cells were then fixed-permeabilized (30 min at 4°C) before intracellular FoxP3 labeling (30 min at 4°C).

Labeled cells were analyzed using a Cytoflex LX apparatus flow cytometer (Beckman Coulter<sup>®</sup> France). Results were analyzed using Kaluza Flow Cytometry software 2.1 (Beckman Coulter<sup>®</sup>).

#### Immunochemistry

Paraffin-embedded tissue sections ( $5\,\mu m$ ) were obtained on the histology platform of the Biscem collaborative services unit at the University of Limoges (Inserm 042, CNRS 2015; Hospital University Center of Limoges) and were deparaffinized as follows: slides were immersed successively in xylene twice for 3 min, 3 times for 3 min in 100% ethanol, once for 3 min in 95% ethanol, and 3 times in PBS for 5 min. Then, slides were immersed in citrate buffer pH 7 and heated 4 times for 5 min 40 s in a microwave at 800 W. For T-cell staining, a primary antibody against CD3 (SP7; Abcam®) was used. Primary antibody revelation was performed using the Zytochem Plus (HRP) Anti-Rabbit (DAB) kit (Zytomed systems®) following the supplier's instructions. Image acquisition was performed using Nanozoomer 2.0RS Hamamatsu Photonics and NDP.scan software.

#### **Immunofluorescence**

Immunofluorescent staining was performed on 8 µm tissue sections cryostained from OCT-frozen blocks. The slides were fixed in cold acetone (–20°C) for 20 min before a saturation step in PBS 3% BSA for 45 minutes. The labeling mix contained B220-FITC (REA755; Miltenyi Biotec®) and CD3-PE (REA641; Miltenyi Biotec®) antibodies diluted 1:100 and 1:167, respectively, and was incubated overnight at 4°C in the dark. The following day, DAPI staining was performed at BD Biosciences®. Slides were mounted and scanned using an epifluorescence microscope Nikon NiE (Nikon®). Labels were analyzed and quantified using QPath software.

#### **Bulk RNA sequencing**

For RNA sequencing, B-cells (CD19+) and T-cells (CD3+/CD4+ and CD3+/CD8+) were sorted on a FACSAriall flow cytometer (BD Biosciences) from the spleen of 10-month-old  $Cd19^{Cre}$  (n = 5) and  $Myd88^{L252P}$  (n = 5) mice. Total mRNA was extracted from purified B-cells, CD4+T-cells, and CD8+T-cells using the RNeasy Mini Kit (QIAGEN). RNAseq libraries and sequencing were performed with Integragen Society (Evry). Alignment was performed on the GRCm39

version of the mouse genome with the STAR package3. Counting reads per gene was carried out with htseq-count of STAR, resulting in an expression table of 56475 annotated genes by the Ensembl genome browser (https://www.ensembl.org/index.html). Then, gene filtering and differential analysis were carried out with EdgeR (https://bioconductor.org/packages/release/bioc/html/edgeR.html and 4). A set of 14444, 14523, and 14334 was selected after gene filtering for CD19-, CD4-, and CD8-positive cells, respectively. Differential analysis was carried out using the exact test function of EdgeR for a difference in the mean between two groups of negative binomial random variables. Clustering and heatmaps were performed with LPS (S Mareschal, https://CRAN.R-project.org/package=LPS). Gene set enrichment analysis was performed with GSEA software (GSEA v4.3.2 for Window, https://data.broadinstitute.org/gseamsigdb/gsea/software/desktop/4.3/).

#### Cytokine production assay

Cytokine production levels were analyzed by flow cytometry. A total of 2 million cells were cultured in complete RPMI medium (Eurobio Scientific) supplemented with 10% of FBS, 2 mM of L-Glutamine, 1% of Na pyruvate, 100 U/mL of penicillin, and 100 µg/mL of streptomycin (Thermo Fisher Scientific) in 24-well plates. In each well, 4 µL of cocktail containing PMA/ionomycin + Brefeldin A (Biolegend) was added, as well as 2 µL of Monensin (Biolegend). Cells were cultured for 6 h at 37°C, 5% CO<sub>2</sub>. Cells were then harvested and stained with surface CD19, CD3, CD4, CD8, and CD25 antibodies, followed by fixation and permeabilization using a commercial cytofix/cytoperm kit (BD Biosciences) at 4°C for 30 min. Subsequently, intracellular FoxP3, IL-2, IFNy, Granzyme B, IL-10, IL-6, and TNFα were stained at 4°C for another 30 min before proceeding to flow cytometry. Cells with no stimulation were set as negative controls. Antibodies used for the flow cytometry are detailed in the Supporting Information S2: Materials and Methods.

#### Multiplex cytokine profiling by flow cytometry

Cytokine secretion levels of IL-2, IFNy, IL-10, IL-6, and TNF $\alpha$  in serum were quantified by flow cytometry using LEGENDplex<sup>TM</sup> beadbased multiplex assays (Biolegend). Cytometry data were analyzed using LEGENDplex<sup>TM</sup> Data Analysis Software. To normalize results to the amount of total protein in each serum sample, a BCA assay was carried out using the Pierce<sup>TM</sup> BCA Protein Assay Kit (Thermo Scientific<sup>TM</sup>).

#### Ex vivo treatment of splenocytes

For ex vivo treatment, total splenocytes were cultured in T25 flasks for 24 h (2.5 million/mL) in completed RPMI medium as previously described supplemented or not with  $1\,\mu\text{M}$  of Ibrutinib. Before starting culture and at Day 1, cells were stained with surface CD19 and B220 for 30 min, 4°C, and labeled cells were analyzed using a Cytoflex LX (Beckman Coulter). Results were analyzed using Kaluza Flow Cytometry software 2.1 (Beckman Coulter).

#### In vivo treatment

Ibrutinib<sup>®</sup> (IMBRUVICA; Janssen) was administered in the drinking water, and the bottles were changed twice a week. The Ibrutinib<sup>®</sup> solution was prepared as follows: one capsule of Ibrutinib<sup>®</sup> (140 mg) was dissolved into 80 mL of 2-hydroxypropyl-β cyclodextrin 10× solution

buffered at pH = 1.6, and shaken for 1 h. After incubation, the pH of the solution was increased to around 7, yielding the 10× stock solution. Each 100 mL bottle contained 10 mL of lbrutinib  $^{\circledR}$  10× solution + 10 mL of 10% glucose solution (prepared from D-glucose 45% #G8769; Sigma) + 80 mL of H<sub>2</sub>O ultrapure.

#### In vivo CT imaging of the spleen

To measure the spleens,  $100\,\mu\text{L}$  of contrast medium (Exitron Nano 12000; Miltenyi Biotec®) was injected intravenously into each animal. After a 10-min incubation period, the animals were anesthetized with 3% Isofluorane for around 5 min, and then images acquired using the CT scanner (U-SPECT4/CT; MILabs) in the animal care department of the Biscem collaborative services unit at the University of Limoges (Inserm 042, CNRS 2015, Hospital University Center of Limoges). Images were analyzed using pi.MOD software.

#### Statistical analysis

Mann–Whitney two-tailed tests were used for statistical analysis using GraphPad Prism software (\*P < 0.05, \*\*P < 0.01, \*\*\*P < 0.001).

#### **RESULTS**

### Tumor B-cells displayed the hallmarks of an immunomodulatory phenotype

From the age of 6 months, blood samples were taken every month from the animals to monitor the presence of a serum Ig peak by serum protein electrophoresis (SPE). SPE images for one Cd19<sup>Cre</sup> mouse and all  $Myd88^{L25P}$  mice (n = 14) used in this study are shown in Supporting Information S1: Figure S1. All Myd88<sup>L252P</sup> animals showed a serum Ig peak at 10-12 months of age, while control mice did not display any increase in the gamma globulin fraction (Supporting Information S1: Figure S1). This Ig peak was constantly associated with a splenomegaly in  $Myd88^{L25P}$  mice only (n = 6 for  $Cd19^{Cre}$  mice, n = 8 for  $Myd88^{L25P}$  mice, P = 0.0007; Supporting Information S1: Figure S2). For this study, mice were euthanized for analysis when an Ig peak and splenomegaly were both detected. Compared with Cd19<sup>Cre</sup> mice (n = 12), spleen  $Mvd88^{L252P}$  tumor B-cells (n = 8) also showed an abnormally activated phenotype characterized by the overexpression of the activation markers CD80 and CD86 (P = 0.0003; Figure 1A) that correlated with the constitutive activation of NF-kB in presence of the  $Myd88^{L252P}$  mutation. Moreover, spleen tumor B-cells (n = 10) strongly overexpressed PD-L1 when compared with normal B-cells (n = 10) (P < 0.0001; Figure 1B). In addition,  $Myd88^{L252P}$  B-cells (n = 13) partially lost MHC class II expression (P = 0.0011; Figure 1C). We also characterized the cytokine production at the tumor level in the spleen by flow cytometry. We found an increased production of proinflammatory cytokines like IL-6 (P = 0.0025), TNF $\alpha$  (P = 0.0159), and INFy (P = 0.0173) as well as immunosuppressive cytokines like IL-10 (P = 0.0025) in B-cells, clearly demonstrating that  $Myd88^{L252P}$ B-cells showed an immunomodulatory phenotype (Figure 1D,E). Analysis of the secretion of these cytokines in blood samples revealed a significant increase in IL-6 (P = 0.0321) and IL-10 secretion (P < 0.0001) in  $Myd88^{L252P}$  mice (Figure 1F,G). No difference was found for IFN $\!\gamma\!$  , while an upward trend was observed for TNF $\!\alpha$ secretion (P = 0.0617; Figure 1F).

RNA sequencing (RNAseq) was performed on sorted CD19<sup>+</sup> B-cells from both  $Myd88^{L252P}$  (n = 5) and control  $Cd19^{Cre}$  mice (n = 5). A total of 3671 genes were differentially expressed between

25729241, 2025, 10, Downloaded from https://onlinelibrary.wiley.com/doi/10.1002/hem3.70231, Wiley Online Library on [03/11/2025]. See the Terms and Conditions (https://onlinelibrary.wiley.com/terms-and-conditions) on Wiley Online Library for rules of use; OA articles are governed by the applicable Creative Commons License

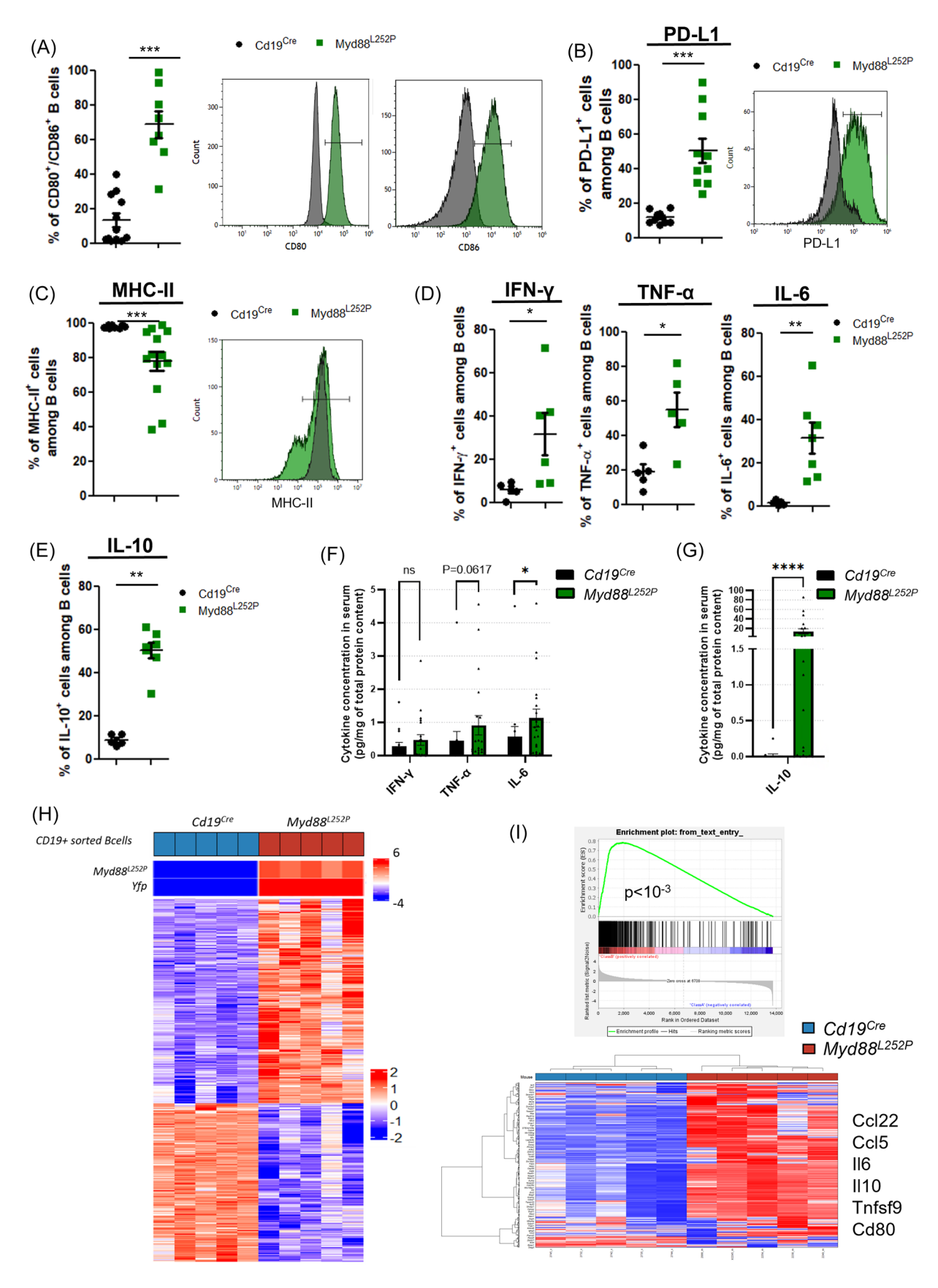


FIGURE 1 (See caption on next page).

FIGURE 1 Tumor B-cells from Myd88<sup>L252P</sup> mice presented an immunomodulatory phenotype. (A) The frequency of activated B-cells (CD80+, CD86+) from the CD19<sup>+</sup> splenic population of  $Cd19^{Cre}$  (n = 12) and  $Myd88^{L252P}$  mice (n = 8) obtained by flow cytometry analysis is shown in the left panel. The middle panel shows an example of a single-parameter histogram showing the mean fluorescence intensity of the CD80 marker for Cd19<sup>Cre</sup> (gray) and Myd88<sup>L252P</sup> (green) groups. The right panel shows an example of a single-parameter histogram showing the mean fluorescence intensity of the CD86 marker for Cd19<sup>Cre</sup> (gray) and Myd88<sup>L252P</sup> (green) groups. (B) The frequency of PD-L1-positive cells among the B220<sup>+</sup> splenic population of Cd19<sup>Cre</sup> (n = 10) and Myd88<sup>L252P</sup> mice (n = 10) obtained by flow cytometry analysis is shown in the left panel. The right panel shows an example of a single-parameter histogram showing the mean fluorescence intensity of the PD-L1 marker for Cd19<sup>Cre</sup> (gray) and Myd88<sup>L252P</sup> (green) groups. (C) The frequency of MHC-II-positive cells among the B220<sup>+</sup> splenic population of Cd19<sup>Cre</sup> (n = 10) and Myd88<sup>L252P</sup> mice (n = 13) obtained by flow cytometry analysis is shown in the left panel. The right panel shows an example of a single-parameter histogram showing the mean fluorescence intensity of the MHC-II marker for  $Cd19^{Cre}$  (gray) and  $Myd88^{L252P}$  (green) groups. (D) Frequency of IFNy-, TNF $\alpha$ -, and IL-6-positive cells among the CD19<sup>+</sup> splenic population obtained by flow cytometry analysis.  $Cd19^{Cre}$  n = 5;  $Myd88^{L252P}$  n = 7. (E) Frequency of IL-10-positive cells among the CD19<sup>+</sup> splenic population obtained by flow cytometry analysis. Cd19<sup>Cre</sup> n = 5; Myd88<sup>L252P</sup> n = 7. (F) Analysis of IFNγ, TNFα, and IL-6 secretion levels in blood samples from Cd19<sup>Cre</sup> (n = 14) and  $Myd88^{L252P}$  mice (n = 20). (G) Analysis of the IL-10 secretion level in blood samples from  $Cd19^{Cre}$  (n = 14) and  $Myd88^{L252P}$  mice (n = 20). (H) mRNA sequencing analysis of  $Cd19^{Cre}$  and  $Myd88^{L252P}$  mouse spleen CD19+ sorted B-cells. Color heatmap of the expression of  $Myd88^{L252P}$  and Yfp and for differentially expressed genes (DEG) between  $Cd19^{Cre}$  and  $Myd88^{L252P}$  B-cells.  $Cd19^{Cre}$  n = 5;  $Myd88^{L252P}$  n = 5. (I) Gene set enrichment analysis (GSEA) of DEG from splenic CD19 sorted B-cells of Cd19<sup>Cre</sup> and Myd88<sup>L252P</sup> mice, revealing a B-regulatory signature<sup>30</sup> in Myd88<sup>L252P</sup> mice. For all panels, Mann-Whitney test P < 0.05, P < 0.01, and P < 0.001 are indicated by \*, \*\*, and \*\*\*, respectively.

Myd88<sup>L252P</sup> and Cd19<sup>Cre</sup> B-cells, with a false discovery rate (FDR) ≤1% (Figure 1H and Supporting Information S3: Table S1). Specific quantification of reads aligned either to the Yfp sequence or harboring the Myd88<sup>L252P</sup> mutation first demonstrated and confirmed the expression of the transgene in purified Myd88<sup>L252P</sup> splenic B-cells, with virtually no reads detected for B-cells from Cd19<sup>Cre</sup> control mice (Figure 1H). Consequently, Yfp and Myd88<sup>L252P</sup> were among the top three in terms of fold change and significance. Gene set enrichment analysis (GSEA) showed that Myd88<sup>L252P</sup> regulated genes included E2f1 and plasma cell signatures (Supporting Information S1: Figure S3). The E2f1 signature is very likely to reflect the increase in cell proliferation. The plasma cell signature is likely to be related to the expected lymphoplasmacytic aspect of Myd88<sup>L252P</sup> B-cell tumors. This RNAseq analysis also revealed a B-regulatory (Breg) signature with an enrichment in some immunoregulatory genes such as II10 or Lag3 as well as genes reflecting the interferon response such as Ifi27 or Ifi44 or the activation and proliferation status of cells such as Cd80, Il2ra (CD25), or Mki67 (Figure 11) or NF-κB activation such as Fas, Ebi3, or Traf1.

Thus, Myd88<sup>L252P</sup> B-cell tumors clearly showed an activated, plasma cell, and immunoregulatory phenotype, the latter raising the question of alterations in T-cells.

# The global proportion of immune B and T compartments was disturbed in the spleen of Myd88<sup>L252P</sup> mice

To study the consequences of such immunomodulatory phenotypes of B-cells on the tumor immune microenvironment and particularly on the T-cell compartment, we first performed an immunochemistry (IHC) staining with a CD3 antibody. In comparison with the normal spleen from Cd19<sup>Cre</sup> control mice, we observed a decrease in CD3 labeling in the T-cell area in Myd88<sup>L252P</sup> mice (Figure 2A). The evaluation of the absolute number of T-cells in the spleen confirmed the IHC results, with a strong decrease in the number of CD3<sup>+</sup> T-cells in Myd88 L252P mice (n = 9) compared to control mice (n = 11)(P = 0.0004; Supporting Information S1: Figure S4A). Using flow cytometry, we evaluated the percentages of lymphoid cells in the spleens of  $Cd19^{Cre}$  control (n = 5) and  $Myd88^{L252P}$  mice (n = 5)(Supporting Information S1: Figure S4A). We confirmed an increase in the percentage of CD19<sup>+</sup> B-cells in tumors, representing 90% of spleen lymphocytes (P = 0.0076) versus 60% under normal conditions, which was associated with a strong decrease in  $CD4^+$  (P = 0.0048) and CD8<sup>+</sup> (P = 0.0120) T-cells (n = 9 for  $Cd19^{Cre}$  mice and n = 6 for

Myd88<sup>L252P</sup>; Supporting Information S1: Figure S4B). As expected, these first results confirm that Myd88<sup>L252P</sup> B-cells invaded the spleen and disturbed the T-cell immune compartment. To better analyze the B- and T-cell distribution in the spleen tissue, we performed doubleimmunofluorescence labeling with anti-CD3 and anti-B220 mAbs conjugated to PE and FITC, respectively. In Cd19<sup>Cre</sup> control mice, we observed a very close but distinct spatial distribution of B- and T-cells, corresponding to the expected T- and B-cell areas in a normal spleen (Figure 2B-E), with B-cells organized in follicles and T-cells below them (Figure 2C,D). In Myd88<sup>L252P</sup> tumor spleens, localization of B and T-cells was disorganized with the presence of T-cells within the B-cell area, suggesting migration of T-cells into the tumor area (Figure 2F-I). This presence of CD3-expressing T-cells in the B-cell tumor strongly indicates an inflamed phenotype Myd88<sup>L252P</sup> B-cell tumors (Figure 2G-I), which suggests a pre-existing anti-tumor response that has been locally inhibited by immunosuppressive mechanisms.31

## T-cells showed features of an activated anti-tumor immune response

Given the intermixed topographies of T-cells and Myd88<sup>L252P</sup> tumor B-cells, CD4 and CD8 populations were further characterized by flow cytometry. Double CD44-CD62L staining of CD4 and CD8 T-cells enables identification of three subpopulations: naive (CD62L+ CD44-), memory (CD62L+ CD44+), and effector T-cells CD44<sup>+</sup>) (Supporting Information S1: Figure S5)<sup>32</sup>. In  $Myd88^{L252P}$  mice (n = 13), mainly CD4<sup>+</sup> but also CD8<sup>+</sup> subsets showed a decrease in naive and memory compartments, concomitant with a significant increase in effector T-cells (P < 0.001; Figure 3A,B). This increase was associated with activation of both CD4<sup>+</sup> and CD8<sup>+</sup> populations, as revealed by increased expression of CD134 and CD137 markers (P < 0.0001; Figure 3C,D). We then investigated the activity of T-cells at the functional level. Ex vivo experiments for the measurement of cytokine production were performed on splenocytes from  $Cd19^{Cre}$  (n = 5) and  $Myd88^{L252P}$  mice (n = 5). We first focused our analysis on cytokines known to be responsible for T-cell activation. Regarding CD4<sup>+</sup> T-cells, no difference was observed in IL-2 production between Cd19<sup>Cre</sup> and Myd88<sup>L252P</sup> mice (Figure 3E, left panel). However, we detected an increase in IFN $\gamma$  production in  $Myd88^{L252P}$  mice (P = 0.0079; Figure 3E, right panel). CD8<sup>+</sup> T-cells from Myd88<sup>L252P</sup> mice produced higher amounts of both IL-2 and IFNy (P = 0.0079; Figure 3F left and middle panels) as well as of the granzyme B-type cytotoxic molecule HemaSphere 7 of 17

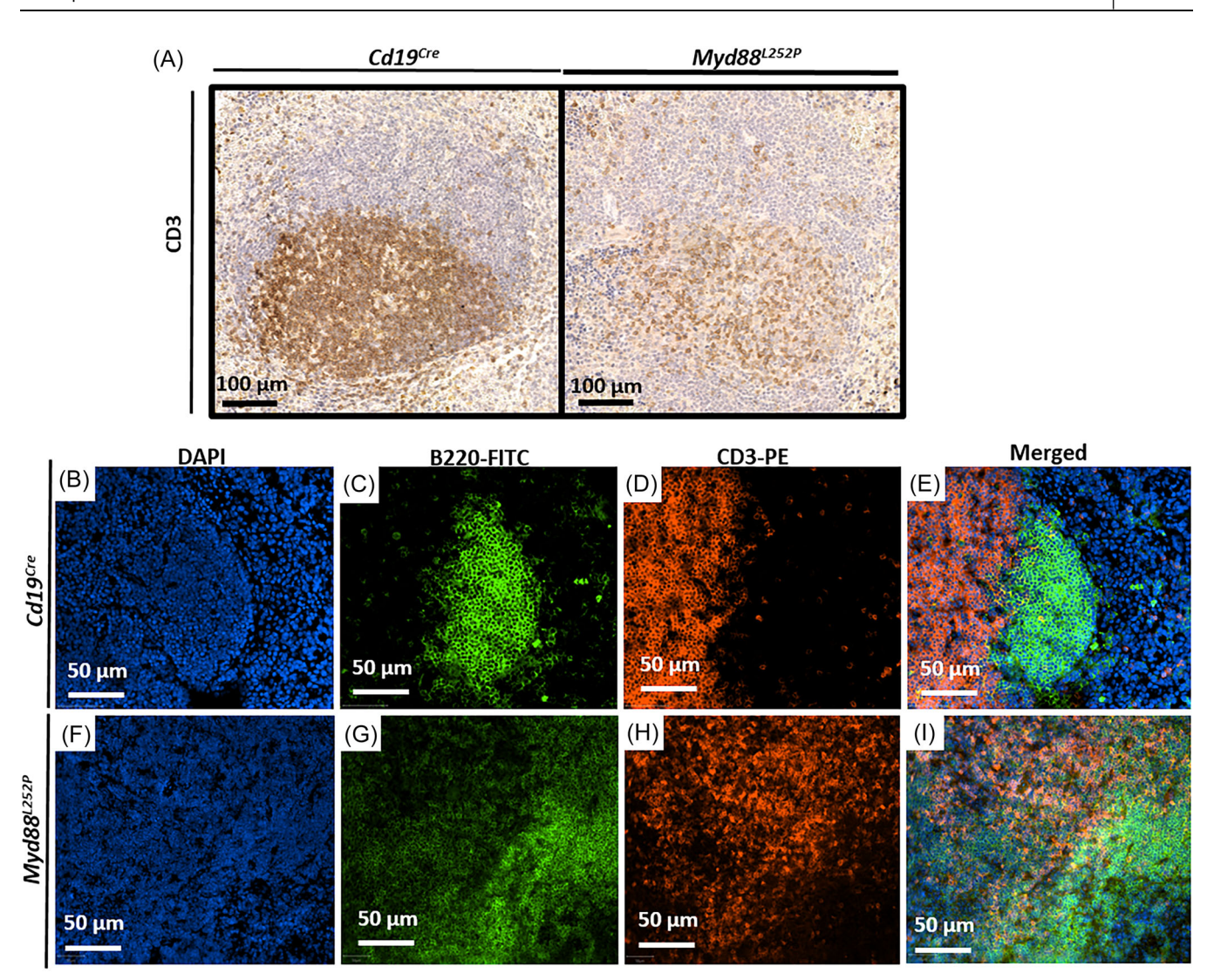


**FIGURE 2** Immunostaining showed a disruption of spleen organization in *Myd88*<sup>L252P</sup> mice. (A) Anti-CD3 labeling was performed on paraffin-embed spleen sections and compared between *Cd19*<sup>Cre</sup> and *Myd88*<sup>L252P</sup> mice. (B, F): DAPI counter stain of *Cd19*<sup>Cre</sup> and *Myd88*<sup>L252P</sup> spleens, respectively. (C, G) B-cells of *Cd19*<sup>Cre</sup> and *Myd88*<sup>L252P</sup> mice are revealed with the anti-B220-FITC antibody. (D, H) T-cells of *Cd19*<sup>Cre</sup> and *Myd88*<sup>L252P</sup> mice are revealed with the anti-CD3-PE antibody. (E, I) Visualization of merged channels (DAPI + FITC + PE).

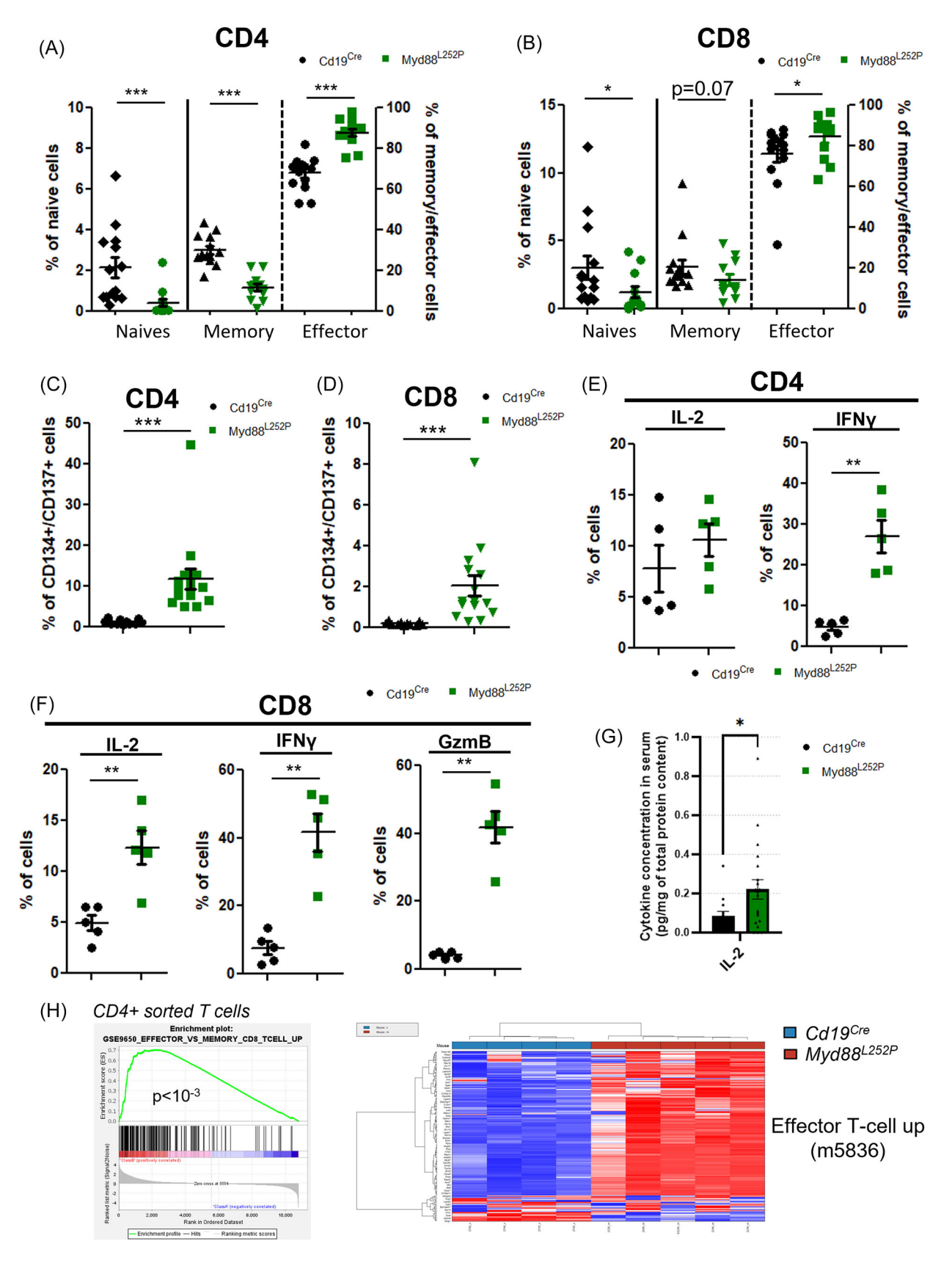
(P = 0.0079; Figure 3F, right panel). Using flow cytometry, we confirmed the increase in IL2 secretion with  $Myd88^{L252P}$  expression (P = 0.0475; Figure 3G).

RNAseq analysis of spleen purified CD4<sup>+</sup> and CD8<sup>+</sup> T-cells from both  $Cd19^{Cre}$  (n=5) and  $Myd88^{L252P}$  mice (n=5) revealed that 5670 and 5426 genes were, respectively, differentially expressed in CD4<sup>+</sup> and CD8<sup>+</sup> populations (Supporting Information S3: Tables S2 and S3 and Supporting Information S1: Figure S6A,B). GSEA analysis confirmed at the molecular level the predominance of effector T-cell differentiation in both CD4+ (Figure 3H) and CD8+ sorted T-cells (data not shown). Even if IL2 was not differentially expressed at the mRNA levels, the IFN $\gamma$  gene was strongly overexpressed by both CD4+ and CD8+T-cells (fold change = 4.2 and 3.6, adjusted  $P=5.10^{-4}$  and  $2.10^{-4}$ , respectively).

These results show that T-cells infiltrating WM-like tumors were mainly activated effector T-cells with increased secretion of IL-2, which is in agreement with engagement in an antitumor immune response with the production of activating and cytotoxic cytokines.

### Tumor-infiltrated T-cells were exhausted in *Myd88*<sup>L252P</sup> mice

The immunomodulatory phenotype of B-cells and the involvement of T-cells in an anti-tumor immune response suggested that the tumor must have developed mechanisms to limit T-cell activity. We further characterized T-cells by studying surface expression of the four main checkpoint molecules that reflect T-cell exhaustion: Programmed cell Death-1 (PD-1), Cytotoxic T-Lymphocyte-Associated protein-4 (CTLA-4), T-cell Immunoglobulin and Mucin containing protein-3 (TIM-3), and Lymphocyte-Activation Gene-3 (LAG-3). Since B-cells strongly expressed the PDL-1 molecule, we first investigated PD-1 expression on CD4- and CD8-expressing T-cells. We found a clear overexpression of PD-1 on the surface of both T-cell populations, with about 80% of CD4 $^+$  or CD8 $^+$  T-cells expressing this marker in  $Myd88^{L252P}$  mice (n=11), compared with 15% and 5%, respectively, for CD4 $^+$  and CD8 $^+$  cells in  $Cd19^{Cre}$  control mice (n=12) (P < 0.0001; Figure 4A and Supporting Information S1: Figure S7A). We completed



2572924, 1, 2025, 10, Downloaded from https://onlinelibrary.wiley.com/doi/10.1002/hem3.70231, Wiley Online Library on [03/11/2025], See the Terms and Conditions (https://onlinelibrary.wiley.com/terms-and-conditions) on Wiley Online Library for rules of use; OA articles are governed by the applicable Creative Commons License

FIGURE 3 (See caption on next page).

HemaSphere 9 of 17

FIGURE 3 Tumor-infiltrated T-cells from  $Myd88^{L252P}$  tumors presented an overactivated phenotype. (A) Frequencies of naive (CD62L<sup>+</sup> CD44<sup>+</sup>), memory (CD62L<sup>+</sup> CD44<sup>+</sup>), and effector (CD62L<sup>-</sup> CD44<sup>+</sup>) CD4<sup>+</sup> T-cells obtained by flow cytometry analysis are compared between  $Cd19^{Cre}$  (n = 14) and  $Myd88^{L252P}$  (n = 13) mice. (B) Frequencies of naive (CD62L<sup>+</sup> CD44<sup>+</sup>), memory (CD62L<sup>+</sup> CD44<sup>+</sup>), and effector (CD62L<sup>-</sup> CD44<sup>+</sup>) CD8<sup>+</sup> T-cells obtained by flow cytometry analysis are compared between  $Cd19^{Cre}$  (n = 14) and  $Myd88^{L252P}$  (n = 13) mice. (C) Frequency-activated T-cells (CD134+, CD137+) from CD4<sup>+</sup> T-cells of  $Cd19^{Cre}$  (n = 11) and  $Myd88^{L252P}$  (n = 15) mice obtained by flow cytometry. (D) Frequency-activated T-cells (CD134+, CD137+) from CD8 + T-cells of  $Cd19^{Cre}$  (n = 11) and  $Myd88^{L252P}$  (n = 15) mice obtained by flow cytometry. (E) Frequency of IL-2- and IFNy-positive cells from CD4 + T-cells of  $Cd19^{Cre}$  (n = 5) and  $Myd88^{L252P}$  (n = 5) mice obtained by flow cytometry. (F) Frequency of IL-2-, IFNy-, and GzmB-positive cells from CD8 + T-cells of  $Cd19^{Cre}$  (n = 5) and  $Myd88^{L252P}$  (n = 5) mice obtained by flow cytometry.  $Cd19^{Cre}$  (n = 5) Analysis of IL-2 secretion levels in blood samples from  $Cd19^{Cre}$  (n = 14) and  $Myd88^{L252P}$  mice (n = 20). (H) Gene set enrichment analysis (GSEA) from differentially expressed genes (DEG) CD4+ sorted T-cells from  $Cd19^{Cre}$  and  $Myd88^{L252P}$  mice. Left panel, GSEA plot of GSE9650\_EFFECTOR\_VS\_MEMORY\_CD8\_T\_CELL\_UP in splenic CD4<sup>+</sup> T-cells from  $Cd19^{Cre}$  compared to  $Myd88^{L252P}$  mice. Color heatmap after GSEA analysis showing the effector T-cell up-signature in splenic sorted CD4 + T-cells of  $Myd88^{L252P}$  mice (n = 5) compared to splenic sorted CD4 + T-cells of  $Cd19^{Cre}$  mice (n = 5). For all panels, Mann-Whitney P < 0.01 and P < 0.001 are indicated by \*\* and \*\*\*\*, respectively.

this analysis by exploring other known markers of exhaustion. CTLA-4 expression was more heterogeneous, but overexpression was found on both CD4<sup>+</sup> and CD8<sup>+</sup> cells (P = 0.0051; Figure 4B and Supporting Information S1: Figure S7B). Finally, expression of TIM-3 and LAG-3 was much greater on both CD4 and CD8 T-cells from spleen  $Myd88^{L252P}$  mice (P < 0.001; Figure 4C,D and Supporting Information S1: Figure S7C,D). The expression of these four exhaustion markers was almost absent in T-cells from control mice. Consistently, GSEA analysis of RNAseq of sorted CD4+ and CD8+ T-cells from  $Myd88^{L252P}$  (n = 5) and  $Cd19^{Cre}$  mice (n = 5) revealed an exhausted immune signature with overexpression of Lag3, Pdcd1, and Ctla4 genes associated with the expression of the  $Myd88^{L252P}$  mutation (Figure 4E).

These results demonstrate the presence of CD4 and CD8 T-cell exhaustion in the tumor of our *Myd88*<sup>L252P</sup> mouse model. This exhaustion impaired the anti-tumor immune response, and appeared to be partly caused by the tumor cells themselves, which displayed an immunosuppressive phenotype.

### Increase of the regulatory T-cell population in *Myd88*<sup>L252P</sup> mice

Known to be potent mediators of inhibition of the T-cell immune response, we then focused on regulatory T-cells (Tregs). In mice, the Treg lineage is related to the expression of the transcription factor Foxp3 and phenotypically, murine Tregs can be defined by the simultaneous expression of CD4, CD25, and FoxP3 markers. 34,35 Using flow cytometry, we found a significantly increased proportion of CD25<sup>+</sup>/FoxP3<sup>+</sup> cells among the CD4<sup>+</sup>, T-cells in  $Myd88^{L252P}$  mice (n = 17), with an average of 20% of CD25<sup>+</sup>/FoxP3<sup>+</sup> cells among CD4<sup>+</sup> (Treg-like) versus 10% in healthy spleens (P < 0.0001; Figure 5A). We demonstrated that in the  $Myd88^{L252P}$  mice (n = 5), those Treg-like produced higher levels of IL-6 and IL-10 than in  $Cd19^{Cre}$  mice (n = 5) (P = 0.0079; Figure 5B,C). As previously reported, TIM-3 enhances the suppressive function of Treg cells.<sup>37</sup> We therefore studied the expression of this immunoregulatory protein in Myd88<sup>L252P</sup> mice. We also found a marked increase in the percentage of Treg-like expressing the TIM-3 marker in tumors, when compared with normal splenic tissue (P = 0.0079; Figure 5D). TIM-3 expression by Tregs correlated with an increase in IL-10<sup>+</sup> production compared with TIM-3 neg Tregs, supporting the maintenance of this immunosuppressive microenvironment in the spleens of  $Myd88^{L252P}$  mice (P = 0.0079, n = 5; Figure 5E). GSEA analysis of RNAseg of sorted CD4<sup>+</sup> T-cells confirmed a Treg signature with an enrichment of upregulated genes such as II10, Ctla4, and Havcr2, correlated with the B-cell expression of Myd88<sup>L252P</sup> (Figure 5F).

Altogether, these data highlight an additional mechanism of immune escape through the expansion of the  $CD25^+$   $FoxP3^+$   $CD4^+$  Treg-like population expressing the TIM-3 molecule.

### Bone marrow populations are also affected by *Myd88*<sup>L252P</sup> expression

In our Myd88<sup>L252P</sup> model, tumors develop mainly in the spleen. However, the bone marrow is also infiltrated by lymphoplasmacytic B-cells. 11 We then assessed the impact of the Myd88<sup>L252P</sup> expression on bone marrow lymphocyte subsets. We first analyzed the B-cell populations and we confirmed our previously published data with an expansion of CD19<sup>+</sup> CD138<sup>+</sup> IgM<sup>+</sup> plasmocytes in Myd88<sup>L252P</sup> mice (n = 8, P = 0.0242; Supporting Information S1: Figure S8A). This was associated with a significant increase in CD80<sup>+</sup> and CD86<sup>+</sup> B-cell populations in  $Myd88^{L252P}$  mice (n = 6) compared with control  $Cd19^{Cre}$ mice (n = 6) (P = 0.0022; Supporting Information S1: Figure S8B). As in the spleen, we found more B-cells that expressed PD-L1 and downregulated MHC-II (P = 0.0095 for PD-L1, P = 0.0159 for MHC-II; Supporting Information S1: Figure S8C,D). Regarding the T-cell compartment by IHC, we detected no difference between control and Mvd88<sup>L52P</sup> bone marrow, with comparable overall CD3<sup>+</sup> cell localization (Supporting Information S1: Figure S8E). Furthermore, using flow cytometry, we confirmed that Myd88<sup>L252P</sup> did not disturb the different subpopulations of naïve, effector, and memory cells for CD4<sup>+</sup> and CD8<sup>+</sup> T-cells (data not shown). Bone marrow T-cells seemed to be less affected by exhaustion than those in the spleen. Indeed, differences observed in the expression of the four exhaustion markers studied (PD-1, CTLA-4, TIM-3, and LAG-3) in the bone marrow CD4+ T-cells of Myd88<sup>L252P</sup> mice were not significant when compared with Cd19<sup>Cre</sup> mice (Supporting Information S1: Figure S8F-I). However, the CD8<sup>+</sup> populations were partly affected, with a significant overexpression of PD-1 and CTLA-4 (P = 0.0016; Supporting Information S1: Figure S8F,G).

Thus, although the phenotype of Myd88<sup>L252P</sup> B-cell tumors was similar between the spleen and the bone marrow, T-cells were affected differently, suggesting that T-cell immune surveillance would also be organ-dependent.

## Effect of ibrutinib treatment on the tumor immune microenvironment

Ibrutinib<sup>®</sup>, which is a B-cell inhibitor targeting the Bruton tyrosine kinase, essential for BCR signaling, is currently used in clinical practice for the treatment of patients with chronic lymphocytic leukemia (CLL) or WM. We first evaluated the tumor response to this molecule ex vivo. As shown Figure 6A, whereas tumor B-cells exhausted a spontaneous proliferation in the absence of treatment, we observed a decrease in the absolute number of B-cells after 1 day of treatment with  $1\,\mu\text{M}$  of Ibrutinib (Figure 6A).

We then tested the effect of this molecule in vivo with a cohort of 10  $Myd88^{L252P}$  and 6  $Cd19^{Cre}$  mice that were treated for 42 days with  $Ibrutinib^{®}$  (0.16 mg/mL) in drinking water. At the beginning of

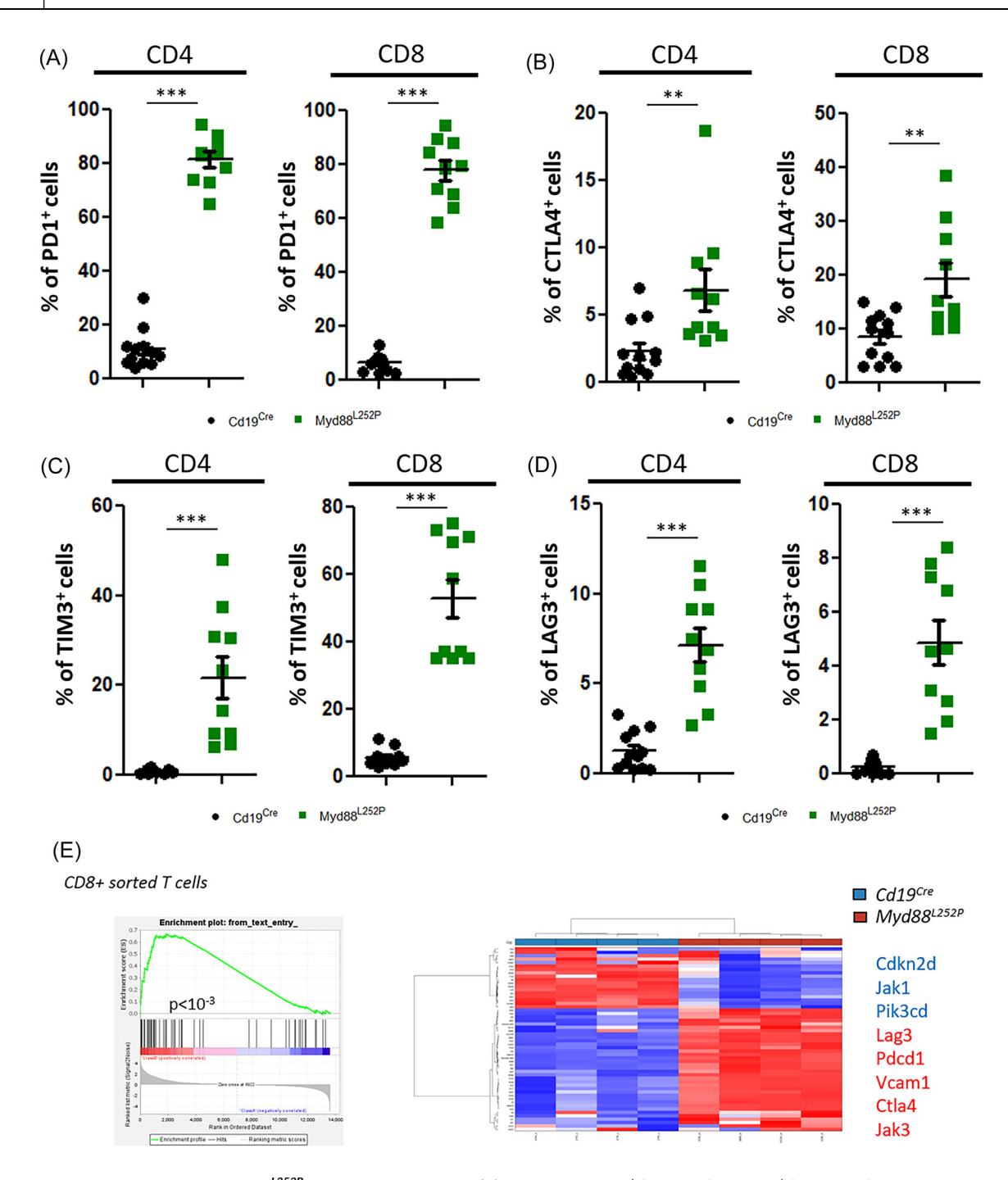
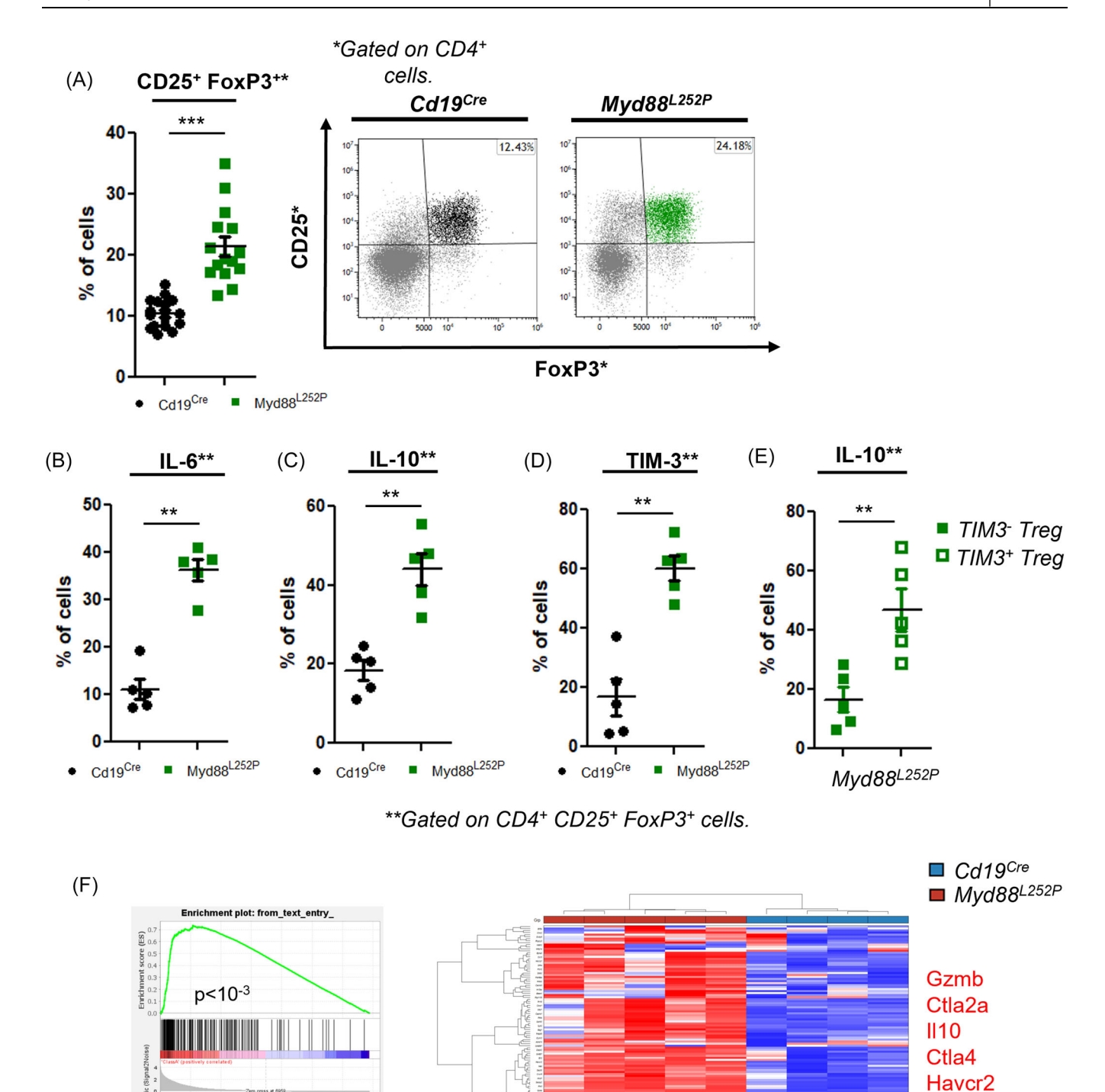


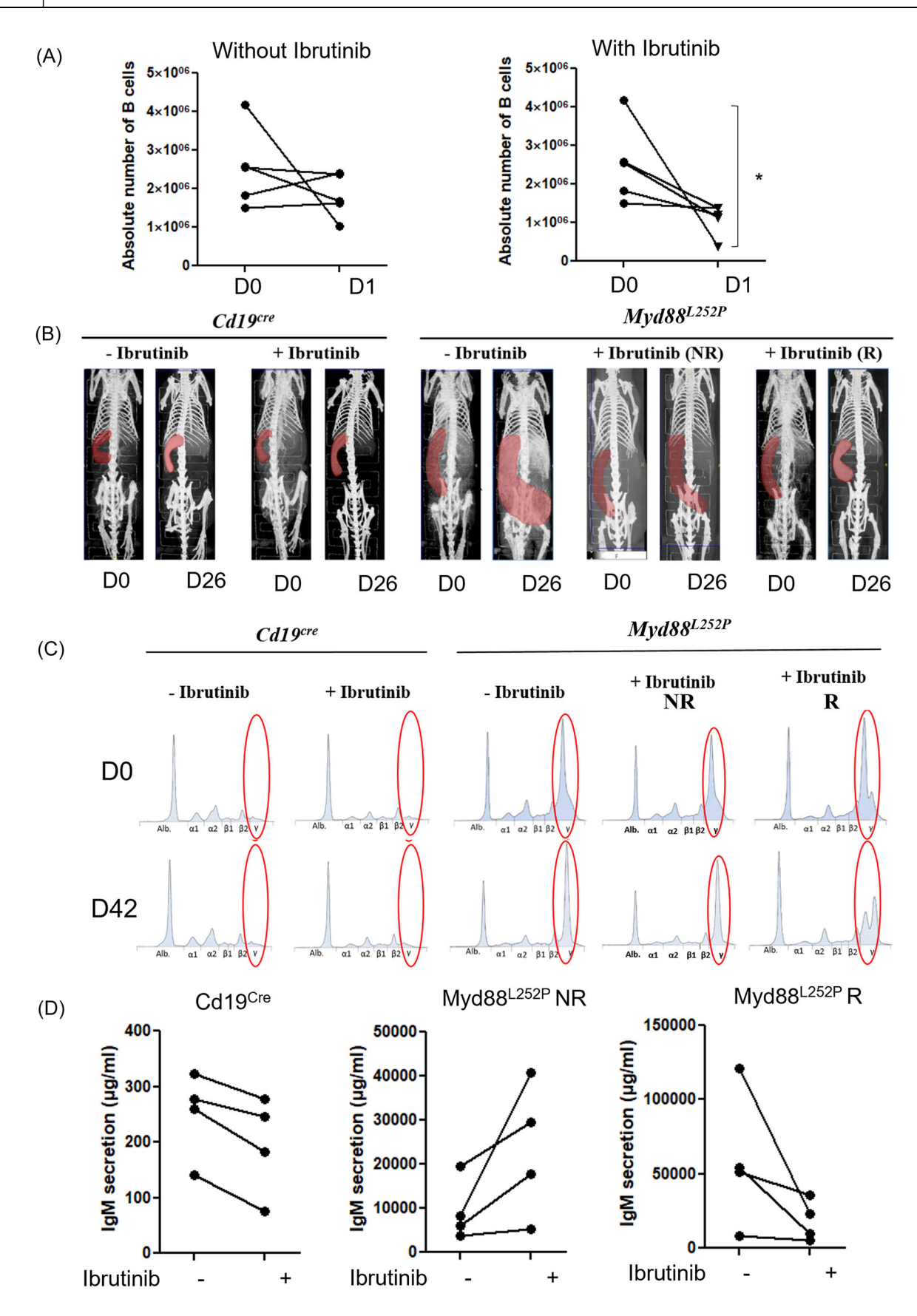
FIGURE 4 Infiltrated T-cells from  $Myd88^{L252P}$  tumors were exhausted. (A) Frequency of CD4<sup>+</sup> (left panel) and CD8<sup>+</sup> (right panel) T-cells expressing PD1 in splenic cells from  $Cd19^{Cre}$  (n = 12) and  $Myd88^{L252P}$  (n = 11) groups by flow cytometry. (B) Frequency of CD4<sup>+</sup> (left panel) and CD8<sup>+</sup> (right panel) T-cells expressing CTLA4 in splenic cells from  $Cd19^{Cre}$  (n = 12) and  $Myd88^{L252P}$  (n = 11) groups by flow cytometry. (C) Frequency of CD4<sup>+</sup> (left panel) and CD8<sup>+</sup> (right panel) T-cells expressing TIM3 in splenic cells from  $Cd19^{Cre}$  (n = 12) and  $Myd88^{L252P}$  (n = 11) groups by flow cytometry. (D) Frequency of CD4<sup>+</sup> (left panel) and CD8<sup>+</sup> (right panel) T-cells expressing LAG3 in splenic cells from  $Cd19^{Cre}$  (n = 12) and  $Myd88^{L252P}$  (n = 11) groups by flow cytometry. (E) Gene set enrichment analysis (GSEA) from differentially expressed gene (DEG) CD8+ sorted T-cells from  $Cd19^{Cre}$  and  $Myd88^{L252P}$  mice. Left panel, GSEA plot of the common CD4/CD8 exhaustion signature in splenic CD8<sup>+</sup> T-cells from  $Cd19^{Cre}$  compared to  $Myd88^{L252P}$  mice. Color heatmap after GSEA analysis showing the T-cell exhaustion signature in splenic Sorted CD8 + T-cells of  $Myd88^{L252P}$  mice (n = 5) compared to splenic sorted CD8 + T-cells of  $Cd19^{Cre}$  mice (n = 5). For all panels, Mann–Whitney test P < 0.05, P < 0.01, and P < 0.001 are indicated by \*, \*\*, and \*\*\*, respectively.

HemaSphere 11 of 17



25729241, 2025, 10, Downloaded from https://onlineibhary.wiley.com/doi/10.1002/hem3.70231, Wiley Online Library on [03/11/2025]. See the Terms and Conditions (https://onlineibrary.wiley.com/terms-and-conditions) on Wiley Online Library for rules of use; OA articles are governed by the applicable Creative Commons. Licensea

FIGURE 5 Abnormal proportion of Tregs associated with a dysregulated anti-inflammatory phenotype supports  $Myd88^{L252P}$  tumor progression. (A) Left panel, frequency of CD25<sup>+</sup> FoxP3<sup>+</sup> Tregs among splenic CD4<sup>+</sup> T-cells from  $Cd19^{Cre}$  and  $Myd88^{L252P}$  mice by flow cytometry. Right panel, example of bi-parametric flow cytometry histograms gated on CD4-positive T-cells for expression of CD25 and FoxP3 in  $Cd19^{Cre}$  (n = 16) and  $Myd88^{L252P}$  mice (n = 17). (B) Frequency of IL-6-positive Tregs in  $Cd19^{Cre}$  (n = 5) and  $Myd88^{L252P}$  (n = 5) mice obtained by flow cytometry analysis. (C) Frequency of IL-10-positive Tregs in the spleen of  $Cd19^{Cre}$  (n = 5) and  $Myd88^{L252P}$  (n = 5) mice obtained by flow cytometry analysis. (E) Frequency of IL-10 positivity among the TIM-3<sup>-</sup> and TIM3<sup>+</sup> Tregs in the spleen of  $Myd88^{L252P}$  (n = 5) mice obtained by flow cytometry analysis. (F) Left panel, gene set enrichment analysis (GSEA) from differentially expressed genes (DEG) CD4+ sorted T-cells from  $Cd19^{Cre}$  and  $Myd88^{L252P}$  mice. Left panel, GSEA plot of Treg up-signature 36 in splenic CD4<sup>+</sup> T-cells from  $Cd19^{Cre}$  compared to  $Myd88^{L252P}$  mice. Right panel, color heatmap after GSEA analysis showing the Treg up-signature in splenic sorted CD4+T-cells of  $Myd88^{L252P}$  mice (n = 5) compared to splenic sorted CD4+T-cells of  $Cd19^{Cre}$  mice (n = 5). For all panels, Mann-Whitney test P < 0.05, P < 0.01, and P < 0.001 are indicated by \*, \*\*, and \*\*\*, respectively.



2572924, 1, 2025, 10, Downloaded from https://onlinelibrary.wiley.com/doi/10.1002/hem3.70231, Wiley Online Library on [03/11/2025], See the Terms and Conditions (https://onlinelibrary.wiley.com/terms-and-conditions) on Wiley Online Library for rules of use; OA articles are governed by the applicable Creative Commons License

FIGURE 6 (See caption on next page).

HemaSphere 13 of 17

**FIGURE 6** Monitoring of the B-cell tumor during Ibrutinib treatment. (A) Ex vivo culture of splenocytes with Ibrutinib treatment. Absolute number of B-cells (CD19+/B220+) without treatment (left panel) and with Ibrutinib (right panel). (B) In vivo CT imaging of  $Cd19^{Cre}$  and  $Myd88^{L252P}$  spleen before Ibrutinib treatment (D0) and 26 days after the beginning of the treatment (D26). (C) Analysis of serum protein electrophoresis before (D0) and at the end of the treatment (D42) from blood samples of  $Cd19^{Cre}$  and  $Myd88^{L252P}$  mice treated (+Ibrutinib) or not with Ibrutinib (-Ibrutinib). The red circle indicates the gamma globulin fraction. Alb: Albumin, α1 and α2: alpha-1 and -2 globulins, β1 and β2: beta-1 and -2 globulins. (D) Analysis of IgM secretion with or without Ibrutinib treatment in blood samples from  $Cd19^{Cre}$  (n = 4) and  $Myd88^{L252P}$  mice (n = 10) divided into two groups: a responder group (R, n = 5) and a nonresponder group (NR, n = 5). For this analysis, each line corresponds to one animal before the treatment (-) or with Ibrutinib treatment (+).

TABLE 1 Criteria for response/nonresponse to Ibrutinib treatment

	Responder group	Nonresponder group
Spleen size	More than 10% reduction	Increase or nonsignificant reduction (less than 10%)
Ig peak Ratio Albumin/ Gammaglobulin	Increased ratio	No change or reduction
Survival during treatment	Yes	No

the treatment, all Myd88<sup>L252P</sup> mice were aged between 9 and 11 months and presented a serum Ig peak with spleen enlargement.

Spleen size was monitored during treatment by CT imaging. One measure was performed before the start of the treatment and the second at D26 (Figure 6B). A blood sample was taken, at the beginning and at the end of the treatment, to monitor the Ig peak by serum protein electrophoresis (one example for each group in Figure 6C). After 42 days of treatment and on the basis of the criteria detailed in Table 1. the 10 Mvd88<sup>L252P</sup>-treated animals were divided into two groups: responder (n = 5) and nonresponder (n = 5). We found that responder mice with a decrease in Ig peak and spleen size during treatment were more likely to survive the 42 days of treatment (Supporting Information S1: Figure S9). ELISA assays were performed with a serum sample for each mouse treated before the start of the treatment (-Ibrutinib) and in the presence of the treatment (+Ibrutinib). The level of Ig peak during treatment correlated with the level of IgM secretion, with a decrease in IgM secretion in the responder group but not in the nonresponder group, which showed an overall increase in Ig peak (Figure 6D and Supporting Information S1: Figure S9C).

At the cellular level, we confirmed the inhibitory effect of Ibrutinib<sup>®</sup> on B-cells by showing that both CD80 and CD86 expression decreased in the responder group, with an intermediate decrease in the nonresponders, compared with the untreated condition (P = 0.0020; Supporting Information S1: Figure S10A).

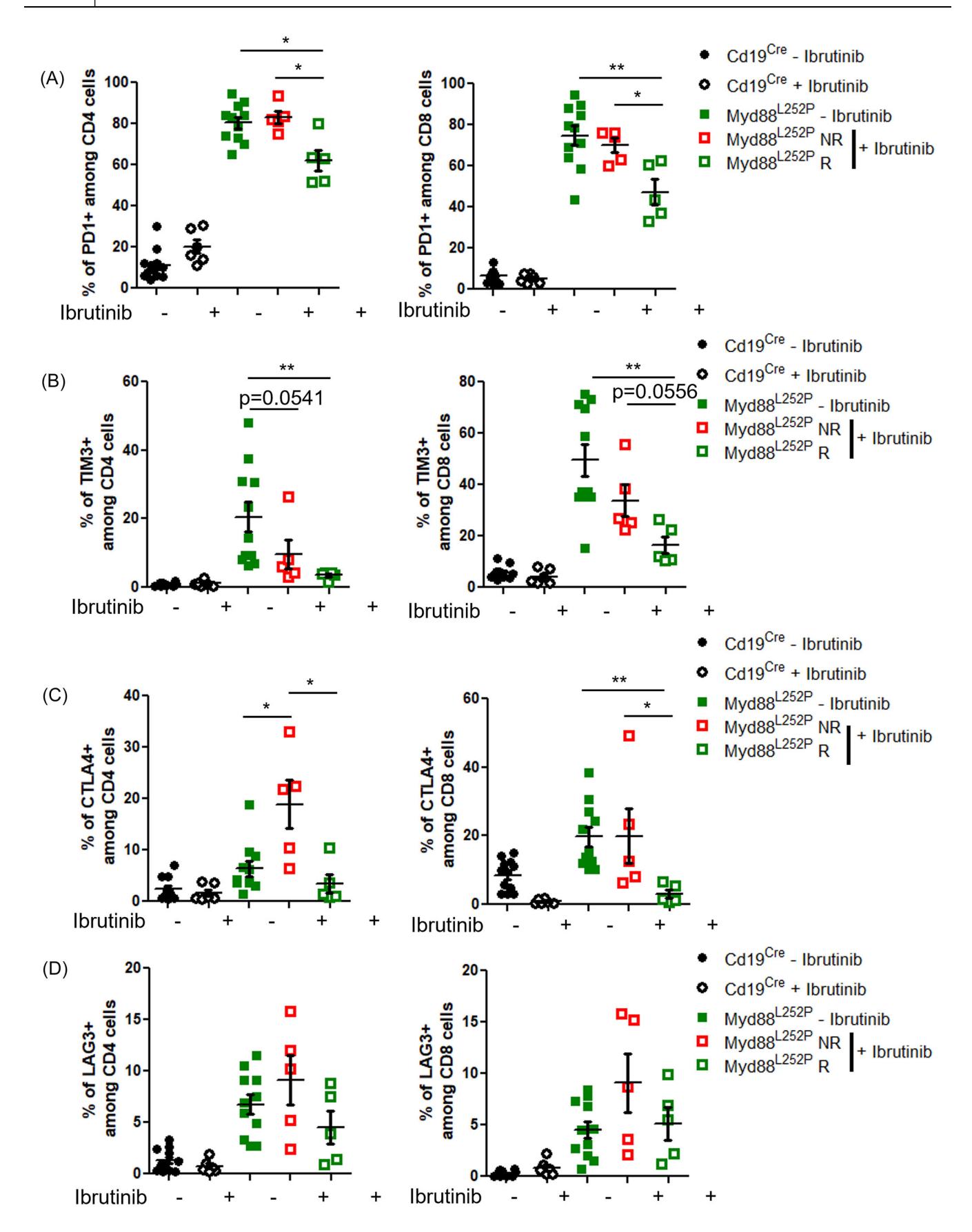
Second, we examined the impact of Ibrutinib<sup>®</sup> treatment on the immune microenvironment particularly on T-cells. During the 42 days of treatment, we first observed no difference in the absolute number of spleen CD3+ T-cells between the untreated group and the responder group (Supporting Information S1: Figure S10A). However, we observed a slight decrease in T-cells for the nonresponder group compared to the other groups, which could explain their poorer response to treatment (Supporting Information S1: Figure 10B). We finally analyzed the effect of Ibrutinib® on the T-cell exhaustion phenotype described before. Regarding the first PD-1, we observed a significant decrease in the surface expression of this marker on CD4<sup>+</sup> T-cells in the responder Myd88<sup>L252P</sup> group compared to untreated mice (P = 0.0127; Figure 7A, left panel). The same result was observed for the CD8<sup>+</sup> population, with a greater decrease in PD-1 expression in the responder group compared with untreated mice (P = 0.0092; Figure 7A, right panel). The nonresponder group showed no change in PD-1 expression in both CD4<sup>+</sup> and CD8<sup>+</sup> T-cells compared with untreated mice, and thus differed significantly

from the responder group (P = 0.0159 and P = 0.0317, respectively, for CD4<sup>+</sup> and CD8<sup>+</sup> populations; Figure 7A). The same results were observed for the expression of TIM-3 in both CD4<sup>+</sup> and CD8<sup>+</sup> T-cells, with a better decrease in the responder group compared with the untreated group (P = 0.0022 for CD4<sup>+</sup>, P = 0.0046 for CD8<sup>+</sup>) and less difference with the nonresponder group (P = 0.0556 for CD8<sup>+</sup> cells) (Figure 7B). The effect of Ibrutinib on CTLA4 expression was less pronounced, with only a decrease in CD8<sup>+</sup> T-cells in the responder group compared with the untreated or the nonresponder group (P = 0.0022 and P = 0.0159, respectively; Figure 7C). Surprisingly, in the nonresponder group, CTLA-4 expression was increased in CD4<sup>+</sup> T-cells (P = 0.0127; Figure 7C).

Finally, treatment did not influence the surface expression of LAG-3 in all treated mice (Figure 7D). Based on these results, Ibrutinib<sup>®</sup> appears to be able to, at least, partially restore T-cell exhaustion by reducing the T-cell expression of PD-1, TIM-3, and CTLA-4 markers.

#### **DISCUSSION**

Evasion of the pressure of immune surveillance is certainly one of the major driving forces in the emergence of B-cell lymphomas. Tumor cells evade immune response by developing an immunosuppressive microenvironment through the dysregulation of immune checkpoint proteins' expression, such proteins being essential in the negative control of activated immune cells. In WM-like lymphoplasmacytic lymphoma of Myd88<sup>L252P</sup> mice, the TME study highlights the development of several immune escape mechanisms. First, tumor B-cells displayed the hallmarks of immunosuppressive B-cells, id-est Bregs. High expression of the CD80 and CD86 activation markers was associated with the overexpression of the PD-L1 molecule and a decrease of MHC-II expression, the latter indicating some loss of tumor-cell immunogenicity. We also confirm this immunosuppressive and inflamed character by showing that tumor cells locally produced large amounts of the immunosuppressive and pro-inflammatory cytokines IL-10, IL-6, and TNFα. This resulted in an increase in IL-6 and IL-10 secretion in the serum of Mvd88<sup>L252P</sup> mice, demonstrating the establishment of an immunosuppressive and inflammatory environment that extended to the spleen. These results are consistent with the constitutive activation of several pathways such as NF-kB and JAK/STAT in our mouse model due to the expression of the Mvd88<sup>L252P</sup> mutation. These first results indicate that of anti-tumor immune response should be disturbed, in particular, T-cell functions. Confirming the inflamed nature of Myd88<sup>L252P</sup> WM-like tumors, we detected migration of T-cells close to the tumor B-cells, suggesting the presence of a pre-existing anti-tumor immune response that was arrested, the exact definition of the immune-inflamed phenotype, as reviewed by Chen and Mellman.<sup>31</sup> Both CD4 and CD8 T-cells were mainly effector T-cells with a decrease in memory T-cells. These T-cells showed hallmarks of an anti-tumor immune response with IL2, IFN $\gamma$ , and TNF $\alpha$  production. In parallel, we also demonstrated the existence of T-cell exhaustion with an overexpression of the four main immune checkpoint molecules PD-1, CTLA-4, TIM-3, and LAG-



257.29241, 2025, 10, Downloaded from https://onlinelibrary.wiley.com/doi/10.1002/hem3.70231, Wiley Online Library on [03/11/2025]. See the Terms and Conditions (https://onlinelibrary.wiley.com/terms-and-conditions) on Wiley Online Library for rules of use; OA articles are governed by the applicable Creative Commons Licenseau Conditions (https://onlinelibrary.wiley.com/terms-and-conditions) on Wiley Online Library for rules of use; OA articles are governed by the applicable Creative Commons Licenseau Conditions (https://onlinelibrary.wiley.com/terms-and-conditions) on Wiley Online Library for rules of use; OA articles are governed by the applicable Creative Commons Licenseau Conditions (https://onlinelibrary.wiley.com/terms-and-conditions) on Wiley Online Library for rules of use; OA articles are governed by the applicable Creative Commons Licenseau Conditions (https://onlinelibrary.wiley.com/terms-and-conditions) on Wiley Online Library for rules of use; OA articles are governed by the applicable Creative Commons Licenseau Conditions (https://onlinelibrary.wiley.com/terms-and-conditions) on Wiley Online Library for rules of use; OA articles are governed by the applicable Creative Commons Licenseau Conditions (https://onlinelibrary.wiley.com/terms-and-conditions) on Wiley Online Library for rules of use; OA articles are governed by the applicable Creative Commons (https://onlinelibrary.wiley.com/terms-and-conditions) on Wiley Online Library for rules of use; OA articles are governed by the applicable Creative Commons (https://onlinelibrary.wiley.com/terms-and-conditions) on Wiley Online Library for rules of use; OA articles are governed by the applicable Creative Commons (https://onlinelibrary.wiley.com/terms-and-conditions) on Wiley Online Library for rules of use; OA articles are governed by the applicable Creative Commons (https://onlinelibrary.wiley.com/terms-and-conditions) on Wiley Online Library for rules of use; OA articles of use; OA articles are governed by the applicable Creative Commons (https://onli

FIGURE 7 (See caption on next page).

HemaSphere 15 of 17

FIGURE 7 Effect of the Ibrutinib on the expression of T-cell exhaustion markers. (A) Frequency of CD4+ (left panel) and CD8+ (right panel) T-cells expressing PD-1 in splenic cells from  $Cd19^{Cre}$  and  $Myd88^{L252P}$  groups with (+,  $Cd19^{Cre}$  n = 6;  $Myd88^{L252P}$  n = 10) or without Ibrutinib treatment (-,  $Cd19^{Cre}$  and  $Myd88^{L252P}$  groups with (+,  $Cd19^{Cre}$  n = 6;  $Myd88^{L252P}$  n = 10) or without Ibrutinib treatment (-,  $Cd19^{Cre}$  n = 6;  $Myd88^{L252P}$  n = 10) or without Ibrutinib treatment (-,  $Cd19^{Cre}$  n = 12;  $Myd88^{L252P}$  n = 11) by flow cytometry. (C) Frequency of CD4+ (left panel) and CD8+ (right panel) T-cells expressing CTLA-4 in splenic cells from  $Cd19^{Cre}$  and  $Myd88^{L252P}$  groups with (+,  $Cd19^{Cre}$  n = 6;  $Myd88^{L252P}$  n = 10) or without Ibrutinib treatment (-,  $Cd19^{Cre}$  n = 12;  $Myd88^{L252P}$  n = 11) by flow cytometry. (D) Frequency of CD4+ (left panel) and CD8+ (right panel) T-cells expressing LAG-3 in splenic cells from  $Cd19^{Cre}$  and  $Myd88^{L252P}$  groups with (+,  $Cd19^{Cre}$  n = 12;  $Myd88^{L252P}$  groups with (+,  $Cd19^{Cre}$  n = 12;  $Myd88^{L252P}$  groups with (+,  $Cd19^{Cre}$  n = 12) or without Ibrutinib treatment (-,  $Cd19^{Cre}$  n = 12) by flow cytometry.

3, associated with an increase in TNF $\alpha$  and d'IL-10 production and with a T-cell-exhausted signature at the RNAseq level. Thus, our mouse model recapitulates what is suspected in WM patients: the presence of the constitutively active mutated MYD88 protein induces the emergence of an immunosuppressive tumor phenotype responsible for T-cell exhaustion with age. <sup>27,38</sup>

Similar to the observations made in WM patients, we demonstrated in our mouse model an increase in the population of CD25+ and FoxP3<sup>+</sup> CD4<sup>+</sup> Tregs-like in splenic tumors.<sup>27</sup> Tregs are immunosuppressive cells, and deregulation of their functions is known to be involved in many cancers. Here, we showed that Tregs-like cells from WM-like tumors overexpressed the anti-inflammatory cytokines IL-10 and IL-6. This is in agreement with a recent study showing, in the Myd88<sup>L252P</sup> mouse model created by Knittel et al. and in patients, the existence of a Treg-mediated immunosuppressive phenotype in WM.<sup>8,39</sup> We also uncovered expansion of TIM-3<sup>+</sup> Tregs-like cells, which secreted higher amounts of immunosuppressive IL-10 cytokine than TIM-3<sup>-</sup> Tregs. It is noteworthy that TIM3-positive Tregs are known to be associated with an unfavorable prognosis in many cancers due to the huge secretion of IL-10.37 Targeting this population would then be a therapeutic prospect for WM. In this sense, Sacco et al. proposed targeting the CD40/CD40L axis after having identified its role in the WM cell-Tregs interaction.<sup>39</sup>

Bone marrow analysis showed that Myd88<sup>L252P</sup> expression from the earliest stages of B-cell development globally affected the B-cell lineage. Indeed, we confirmed our previous data by observation of an infiltration of lymphoplasmacytic cells, 11 which, in this work, are found to show an immunosuppressive B-cell phenotype as in of spleen. However, the T-cell compartment seemed to be less affected than the spleen, suggesting a better anti-tumor immune surveillance in the bone marrow, moderating tumor infiltration in this organ. However, it is noteworthy that bone marrow CD8<sup>+</sup> T-cells overexpressed PD-1 and CTLA-4, indicating that bone marrow Myd88<sup>L252P</sup> tumor B-cells would primarily target the CD8<sup>+</sup> T-cell compartment. Involving contact between the T-cell and its target, the PD-1/PD-L1 and CTLA-4/CD28 axes are the two main immune checkpoints. 40,41 Thus, Myd88<sup>L252P</sup> tumor B-cells would deliver an exhaustion/inhibitory signal to CD8+T-cells when they create an immune synapse.

Ibrutinib, used in the treatment of various B-cell lymphomas, including WM, specifically targets the BCR signaling through inhibition of the BTK enzyme. Several studies on CLL patients have shown that Ibrutinib is able to at least partially restore the T-cell activity by reducing their exhaustion. Indeed, Ibrutinib also targets the T-cell compartment with an immunomodulatory effect by inhibiting IL-2-inducible T-cell kinase (ITK). To Other actions on several kinases have been identified in solid cancers, highlighting BTK as a potential target for solid anti-tumor therapies. For WM, this phenomenon has not yet been identified. Our results show that, *in vivo*, Ibrutinib, in addition to its effect on B-cells and IgM secretion, partially reverses T-cell exhaustion in responding *Myd88*<sup>L252P</sup> mice by reducing the expression of all exhaustion markers. These data suggest that the

direct anti-tumor effect of Ibrutinib is certainly not sufficient on its own and must be combined with reactivation of the immune response.

Ibrutinib<sup>®</sup>'s potential to partially reduce T-cell exhaustion suggests that it would be highly beneficial to use this mechanism in therapy to boost the anti-tumor T-cell immune response, thereby potentiating the inhibitor's effect. Targeting immune checkpoints and especially PD-L1 yielded excellent results in various solid cancers such as those of the lung or colon.<sup>49-51</sup> Apart from Hodgkin lymphomas, such therapies did not show positive results in B-cell lymphomas, especially for those with NF-κB activation.<sup>52</sup> This lack of curative effects in these patients, despite PD-L1 expression by tumor cells in most cases, is to date poorly understood. In WM, such therapies could be of great help because of the MYD88 mutation that constitutively activates NF-κB.

In conclusion, these results highlight the importance of targeting both tumor B-cells and T-cells to induce restoration of the immune response. More importantly, these results reinforce the fact that the deregulation of the NF- $\kappa$ B transcription factor is associated with the establishment of an immunosuppressive environment in B-cell lymphomas, including the development of a B-regulatory phenotype.  $^{16,53}$ 

#### **ACKNOWLEDGMENTS**

We are grateful for the animal, histology, cytometry, and microscopy facilities of the technological platform of the University of Limoges BISCEm (Inserm 042, CNRS 2015, Hospital University Center of Limoges). In particular, we thank Magali Sage for producing the in vivo imaging scanner.

#### **AUTHOR CONTRIBUTIONS**

Quentin Lemasson: Investigation; formal analysis; writing—original draft. Maxime Tabaud: Investigation; formal analysis. Ophélie Téteau: Investigation; formal analysis; funding acquisition. Bastien Carle: Investigation; formal analysis. Mina Chabaud: Investigation; formal analysis. Jean Feuillard: Writing—original draft; formal analysis. Nathalie Faumont: Methodology. Christelle Vincent-Fabert: Methodology; supervision; writing—original draft; writing—review and editing; funding acquisition.

#### CONFLICT OF INTEREST STATEMENT

The authors declare no conflict of interest.

#### DATA AVAILABILITY STATEMENT

The data that support the findings of this study are available from the corresponding author upon reasonable request.

#### **FUNDING**

Q.L. was supported by the "Fondation pour la recherche Médicale (FRM)". C.V.-F., O.T., and J.F. were supported by the "Fondation ARC pour la recherche sur la cancer." C.V.F. was supported by the International Waldenström Macroglobulinemia Foundation. C.V.F. and

O.T. were supported by the "Ligue contre le cancer, comités Haute-Vienne, Corrèze et Creuse."

#### SUPPORTING INFORMATION

Additional supporting information can be found in the online version of this article

#### ORCID

Christelle Vincent-Fabert https://orcid.org/0000-0002-5799-980X

#### REFERENCES

- Gayet M, Leymarie V, Derouault P, et al. Flow cytometry detection of CD138 expression continuum between monotypic B and plasma cells is associated with both high IgM peak levels and MYD88 mutation and contributes to diagnosis of Waldenström macroglobulinemia. Cytometry Part B Clin Cytometry. 2021;102:62-69. doi:10.1002/cyto.b. 21995
- Nguyen-Khac F, Lambert J, Chapiro E, et al. Chromosomal aberrations and their prognostic value in a series of 174 untreated patients with Waldenström's macroglobulinemia. *Haematologica*. 2013;98: 649-654. doi:10.3324/haematol.2012.070458
- Treon SP, Xu L, Yang G, et al. MYD88 L265P somatic mutation in Waldenström's macroglobulinemia. N Engl J Med. 2012;367:826-833. doi:10.1056/NEJMoa1200710
- Gachard N, Parrens M, Soubeyran I, et al. IGHV gene features and MYD88 L265P mutation separate the three marginal zone lymphoma entities and Waldenström macroglobulinemia/lymphoplasmacytic lymphomas. Leukemia. 2013;27:183-189. doi:10.1038/leu.2012.257
- Buske C, Leblond V. How to manage Waldenstrom's macroglobulinemia. Leukemia. 2013;27:762-772. doi:10.1038/leu.2013.36
- Treon SP, Cao Y, Xu L, Yang G, Liu X, Hunter ZR. Somatic mutations in MYD88 and CXCR4 are determinants of clinical presentation and overall survival in Waldenström macroglobulinemia. *Blood*. 2014; 123:2791-2796. doi:10.1182/blood-2014-01-550905
- Simon L, Baron M, Leblond V. How we manage patients with Waldenström macroglobulinaemia. Br J Haematol. 2018;181:737-751. doi:10.1111/bjh.15202
- Knittel G, Liedgens P, Korovkina D, et al. B-cell-specific conditional expression of Myd88<sup>p.L252P</sup> leads to the development of diffuse large B-cell lymphoma in mice. Blood. 2016;127:2732-2741. doi:10.1182/ blood-2015-11-684183
- Sewastianik T, Guerrera ML, Adler K, et al. Human MYD88<sup>L265P</sup> is insufficient by itself to drive neoplastic transformation in mature mouse B cells. Blood Adv. 2019;3:3360-3374. doi:10.1182/ bloodadvances.2019000588
- Schmidt K, Sack U, Graf R, et al. B-cell-specific Myd88 L252P expression causes a premalignant gammopathy resembling IgM MGUS. Front Immunol. 2020;11:602868. doi:10.3389/fimmu.2020.602868
- Ouk C, Roland L, Gachard N, et al. Continuous MYD88 activation is associated with expansion and then transformation of IgM differentiating plasma cells. Front Immunol. 2021;12:641692. doi:10. 3389/fimmu.2021.641692
- Dreyling M, André M, Gökbuget N, et al. The EHA research roadmap: malignant lymphoid diseases. *HemaSphere*. 2022;6:e726. doi:10. 1097/HS9.00000000000000726
- 13. Zhang B, Kracker S, Yasuda T, et al. Immune surveillance and therapy of lymphomas driven by Epstein-Barr virus protein LMP1 in a mouse model. *Cell.* 2012;148:739-751. doi:10.1016/j.cell.2011.12.031
- Vincent-Fabert C, Soubeyran I, Velasco V, et al. Inflamed phenotype of splenic marginal zone B-cell lymphomas with expression of PD-L1 by intratumoral monocytes/macrophages and dendritic cells. *Cell Mol Immunol*. 2019;16:621-624. doi:10.1038/s41423-019-0228-y
- Vincent-Fabert C, Roland L, Zimber-Strobl U, Feuillard J, Faumont N. Pre-clinical blocking of PD-L1 molecule, which expression is down

- regulated by NF-κB, JAK1/JAK2 and BTK inhibitors, induces regression of activated B-cell lymphoma. *Cell Commun Signaling*. 2019;17:89. doi:10.1186/s12964-019-0391-x
- Vincent-Fabert C, Saintamand A, David A, et al. Reproducing indolent B-cell lymphoma transformation with T-cell immunosuppression in LMP1/CD40-expressing mice. Cell Mol Immunol. 2019;16:412-414. doi:10.1038/s41423-018-0197-6
- Görgün G, Holderried TAW, Zahrieh D, Neuberg D, Gribben JG. Chronic lymphocytic leukemia cells induce changes in gene expression of CD4 and CD8 T cells. J Clin Invest. 2005;115:1797-1805. doi:10.1172/JCI24176
- Hilchey SP, De A, Rimsza LM, Bankert RB, Bernstein SH. Follicular lymphoma intratumoral CD4+CD25+GITR+ regulatory T cells potently suppress CD3/CD28-costimulated autologous and allogeneic CD8+CD25- and CD4+CD25- T cells. *J Immunol*. 2007;178: 4051-4061. doi:10.4049/jimmunol.178.7.4051
- 19. Yang Z-Z, Grote DM, Ziesmer SC, et al. IL-12 upregulates TIM-3 expression and induces T cell exhaustion in patients with follicular B cell non-Hodgkin lymphoma. *J Clin Invest*. 2012;122:1271-1282. doi:10.1172/JCI59806
- Riches JC, Davies JK, McClanahan F, et al. T cells from CLL patients exhibit features of T-cell exhaustion but retain capacity for cytokine production. *Blood*. 2013;121:1612-1621. doi:10.1182/blood-2012-09-457531
- 21. Palma M, Gentilcore G, Heimersson K, et al. T cells in chronic lymphocytic leukemia display dysregulated expression of immune checkpoints and activation markers. *Haematologica*. 2017;102: 562-572. doi:10.3324/haematol.2016.151100
- Kiyasu J, Miyoshi H, Hirata A, et al. Expression of programmed cell death ligand 1 is associated with poor overall survival in patients with diffuse large B-cell lymphoma. *Blood*. 2015;126:2193-2201. doi:10.1182/blood-2015-02-629600
- 23. Yin H, Pu N, Chen Q, et al. Gut-derived lipopolysaccharide remodels tumoral microenvironment and synergizes with PD-L1 checkpoint blockade via TLR4/MyD88/AKT/NF-кВ pathway in pancreatic cancer. *Cell Death Dis.* 2021;12:1033. doi:10.1038/s41419-021-04293-4
- Grote DM, Ziesmer SC, Hodge LS, et al. Interactions between PD-1 and PD-L1 and PD-L2 promote malignant B-cell growth in Waldenstrom macroglobulinemia. *Blood*. 2013;122:4334. doi:10. 1182/blood.V122.21.4334.4334
- Jalali S, Price-Troska T, Paludo J, et al. Soluble PD-1 ligands regulate T-cell function in Waldenstrom macroglobulinemia. *Blood Adv.* 2018:2:1985-1997. doi:10.1182/bloodadyances.2018021113
- Kaushal A, Nooka AK, Carr AR, et al. Aberrant extrafollicular B cells, immune dysfunction, myeloid inflammation, and MyD88-mutant progenitors precede Waldenstrom macroglobulinemia. *Blood Cancer Discovery*, 2021;2:600-615. doi:10.1158/2643-3230.BCD-21-0043
- Sun H, Fang T, Wang T, et al. Single-cell profiles reveal tumor cell heterogeneity and immunosuppressive microenvironment in Waldenström macroglobulinemia. J Transl Med. 2022;20:576. doi:10. 1186/s12967-022-03798-6
- Vincent-Fabert C, Fiancette R, Pinaud E, et al. Genomic deletion of the whole IgH 3' regulatory region (hs3a, hs1,2, hs3b, and hs4) dramatically affects class switch recombination and Ig secretion to all isotypes. *Blood*. 2010;116:1895-1898. doi:10.1182/blood-2010-01-264689
- Chauzeix J, Laforêt M-P, Deveza M, et al. Normal serum protein electrophoresis and mutated IGHV genes detect very slowly evolving chronic lymphocytic leukemia patients. *Cancer Med.* 2018;7: 2621-2628. doi:10.1002/cam4.1510
- Shen P, Roch T, Lampropoulou V, et al. IL-35-producing B cells are critical regulators of immunity during autoimmune and infectious diseases. *Nature*. 2014;507:366-370. doi:10.1038/nature12979
- Chen DS, Mellman I. Elements of cancer immunity and the cancerimmune set point. Nature. 2017;541:321-330. doi:10.1038/ nature21349

HemaSphere 17 of 17

Skordos I, Demeyer A, Beyaert R. Analysis of T cells in mouse lymphoid tissue and blood with flow cytometry. STAR Protocols. 2021; 2:100351. doi:10.1016/j.xpro.2021.100351

- 33. Crawford A, Angelosanto JM, Kao C, et al. Molecular and transcriptional basis of CD4<sup>+</sup> T cell dysfunction during chronic infection. *Immunity*. 2014;40:289-302. doi:10.1016/j.immuni.2014.01.005
- Fontenot JD, Gavin MA, Rudensky AY. Foxp3 programs the development and function of CD4+CD25+ regulatory T cells. *Nat Immunol*. 2003;4:330-336. doi:10.1038/ni904
- Josefowicz SZ, Lu L-F, Rudensky AY. Regulatory T cells: mechanisms of differentiation and function. *Annu Rev Immunol*. 2012;30:531-564. doi:10.1146/annurev.immunol.25.022106. 141623
- 36. Edwards CL, Ng SS, de Labastida Rivera F, et al. Human IL-10-producing Th1 cells exhibit a molecular signature distinct from Tr1 cells in malaria. *J Clin Invest*. 2023;133:e153733. doi:10. 1172/JCI153733
- 37. Banerjee H, Nieves-Rosado H, Kulkarni A, et al. Expression of Tim-3 drives phenotypic and functional changes in Treg cells in secondary lymphoid organs and the tumor microenvironment. *Cell Rep.* 2021; 36:109699. doi:10.1016/j.celrep.2021.109699
- Cholujova D, Beke G, Hunter ZR, et al. Dysfunctions of innate and adaptive immune tumor microenvironment in Waldenström macroglobulinemia. Int J Cancer. 2023;152:1947-1963. doi:10.1002/ijc. 34405
- Sacco A, Desantis V, Celay J, et al. Targeting the immune microenvironment in Waldenström macroglobulinemia via halting the CD40/CD40-ligand axis. *Blood*. 2023;141:2615-2628. doi:10.1182/ blood.2022019240
- Qin S, Xu L, Yi M, Yu S, Wu K, Luo S. Novel immune checkpoint targets: moving beyond PD-1 and CTLA-4. Mol Cancer. 2019;18:155. doi:10.1186/s12943-019-1091-2
- Śledzińska A, Menger L, Bergerhoff K, Peggs KS, Quezada SA. Negative immune checkpoints on T lymphocytes and their relevance to cancer immunotherapy. *Mol Oncol*. 2015;9:1936-1965. doi:10. 1016/j.molonc.2015.10.008
- Long M, Beckwith K, Do P, et al. Ibrutinib treatment improves T cell number and function in CLL patients. J Clin Invest. 2017;127: 3052-3064. doi:10.1172/JCI89756

- Parry HM, Mirajkar N, Cutmore N, et al. Long-term ibrutinib therapy reverses CD8+ T cell exhaustion in B cell chronic lymphocytic leukaemia. Front Immunol. 2019;10:2832. doi:10.3389/fimmu.2019.02832
- Solman IG, Blum LK, Hoh HY, et al. Ibrutinib restores immune cell numbers and function in first-line and relapsed/refractory chronic lymphocytic leukemia. *Leuk Res.* 2020;97:106432. doi:10.1016/j. leukres.2020.106432
- Davis JE, Sharpe C, Mason K, Tam CS, Koldej RM, Ritchie DS. Ibrutinib protects T cells in patients with CLL from proliferation-induced senescence. J Transl Med. 2021;19:473. doi:10.1186/s12967-021-03136-2
- Liu Y, Song Y, Yin Q. Effects of ibrutinib on T-cell immunity in patients with chronic lymphocytic leukemia. Front Immunol. 2022;13: 962552. doi:10.3389/fimmu.2022.962552
- Dubovsky JA, Beckwith KA, Natarajan G, et al. Ibrutinib is an irreversible molecular inhibitor of ITK driving a Th1-selective pressure in T lymphocytes. *Blood*. 2013;122:2539-2549. doi:10.1182/blood-2013-06-507947
- Szklener K, Michalski A, Żak K, Piwoński M, Mańdziuk S. Ibrutinib in the treatment of solid tumors: current state of knowledge and future directions. *Cells*. 2022;11:1338. doi:10.3390/cells11081338
- Yu X, Zhai X, Wu J, et al. Evolving perspectives regarding the role of the PD-1/PD-L1 pathway in gastric cancer immunotherapy. *Biochim Biophys Acta*. 2024;1870:166881. doi:10.1016/j.bbadis.2023.166881
- Li Y, Du Y, Xue C, et al. Efficacy and safety of anti-PD-1/PD-L1 therapy in the treatment of advanced colorectal cancer: a metaanalysis. BMC Gastroenterol. 2022;22:431. doi:10.1186/s12876-022-02511-7
- 51. Kumar S, Chatterjee M, Ghosh P, Ganguly KK, Basu M, Ghosh MK. Targeting PD-1/PD-L1 in cancer immunotherapy: an effective strategy for treatment of triple-negative breast cancer (TNBC) patients. *Genes Dis.* 2023;10:1318-1350. doi:10.1016/j.gendis.2022.07.024
- Mulder TA, Wahlin BE, Österborg A, Palma M. Targeting the immune microenvironment in lymphomas of B-cell origin: from biology to clinical application. Cancers. 2019;11:915. doi:10.3390/ cancers11070915
- Auclair H, Ouk-Martin C, Roland L, et al. EBV latency III-transformed B cells are Inducers of conventional and unconventional regulatory T cells in a PD-L1-dependent manner. *J Immunol.* 2019;203:1665-1674. doi:10.4049/jimmunol.1801420